iScience

CellPress
OPEN ACCESS

Article

Acetylation of NDUFV1 induced by a newly synthesized HDAC6 inhibitor HGC rescues dopaminergic neuron loss in Parkinson models

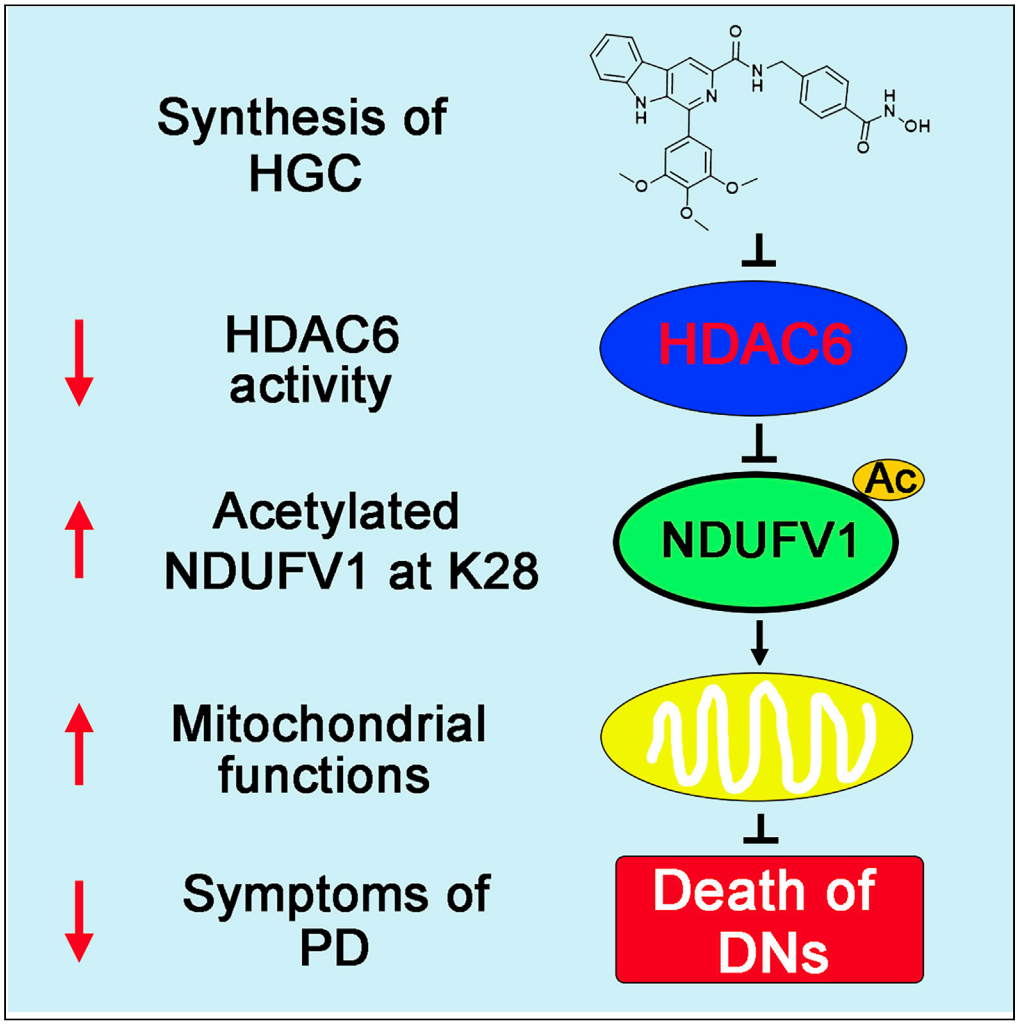

Bing Li, Yinuo Yang, Yuejun Wang, ..., Bolin Lian, Yong Ling, Cheng Sun

lianziadd9@163.com (B.L.)
lyyy111@sina.com (Y.L.)
suncheng1975@ntu.edu.cn (C.S.)

Highlights

HGC is a potent inhibitor for HDACs, especially HDAC1/6

HGC protects dopaminergic neurons and alleviates PD symptoms in PD models

HDAC6/NDUFV1 axis is responsible for transducing its anti-PD activities

HGC holds great therapeutic potentials for treating PD

Li et al., iScience *24*, 102302
April 23, 2021 © 2021 The Author(s).
https://doi.org/10.1016/j.isci.2021.102302

iScience

CellPress
OPEN ACCESS

Article

Acetylation of NDUFV1 induced by a newly synthesized HDAC6 inhibitor HGC rescues dopaminergic neuron loss in Parkinson models

Bing Li,[1,4] Yinuo Yang,[1,4] Yuejun Wang,[1] Jing Zhang,[1] Jie Ding,[1] Xiaoyu Liu,[1] Yan Jin,[2] Bolin Lian,[2,*] Yong Ling,[3,*] and Cheng Sun[1,5,*]

SUMMARY

It has been shown that histone deacetylase (HDAC) inhibitors hold considerable therapeutic potentials for treating neurodegeneration-related diseases including Parkinson disease (PD). Here, we synthesized an HDAC inhibitor named as HGC and examined its neuroprotective roles in PD models. Our results showed that HGC protects dopaminergic neurons from 1-methyl-4-phenylpyridinium (MPP^+)-induced insults. Furthermore, in 1-methyl-4-phenyl-1, 2, 3, 6-tetrahydropyridine (MPTP)-induced PD model mice, HGC application rectifies behavioral defects, improves tyrosine hydroxylase-positive neurons in the midbrain, and maintains mitochondrial integrity and functions. Mechanistically, mass spectrometry data revealed that HGC stimulates acetylation modification at lysine 28 of NDUFV1. Inhibition of HDAC6 by HGC is responsible for this acetylation modification. Functional tests showed that, as well as HGC, NDUFV1 exhibits beneficial roles against MPP^+ injuries. Moreover, knockdown of NDUFV1 abolishes the neuroprotective roles of HGC. Taken together, our data indicate that HGC has a great therapeutic potential for treating PD and NDUFV1 might be a target for developing drugs against PD.

INTRODUCTION

Parkinson disease (PD), the second most common neurodegenerative disorder, affected 6.2 million people in 2015 and resulted in about 117,400 deaths globally (Kalia and Lang, 2015). The most obvious symptoms at early stages of the disease are shaking, rigidity, slowness of movement, and difficulty with walking (Abeliovich and Gitler, 2016). Along with the progression of PD, nonmotor symptoms including loss of smell, rapid eye movement sleep behavior disorder, urinary dysfunction, orthostatic hypotension, constipation, and depression will be diagnosed (Armstrong and Okun, 2020). Moreover, cognitive impairment also is one of the most disabling features of PD at late stages (Armstrong and Okun, 2020). Dopaminergic neuron loss is a hallmark of this neurodegenerative disease (Kalia and Lang, 2015). Dopamine replacement therapies including drugs L-Dopa, apomorphine, pergolide, entacapone, and selegiline are developed and considered as efficient ways for partially controlling motor symptoms of PD (Armstrong and Okun, 2020). In addition, monoamine oxidase (MAO-B) inhibitors are also useful for rectifying motor symptoms at early stages of PD (Armstrong and Okun, 2020). However, recent clinical survey data revealed that these drugs have side effects such as impulse control disorders and dyskinesia when used long term (Armstrong and Okun, 2020; Buck and Ferger, 2010; Poewe et al., 2010). In addition to these chemical drugs, physical intervention such as deep brain stimulation is another way for the treatment of PD (Foltynie and Hariz, 2010). However, none of these strategies can protect dopaminergic neurons from death for long term; and none of the current drug therapies can treat the nonmotor symptoms which greatly affect quality of life of patients with PD. Hence, discovery of new classes of chemicals against PD holds great potentials for providing better therapeutics for PD treatment.

It has been shown that histone acetylation is closely correlated with gene expression. Two kinds of enzymes named as histone acetyltransferases (HATs) and histone deacetylases (HDACs) are responsible for histone acetylation and deacetylation. In general, HATs catalyze the acetylation of lysine residues in histone tails, leading to chromatin relaxation and transcriptional activation; on the contrary, HDACs promote deacetylation,

[1]Key Laboratory of Neuroregeneration of Jiangsu Province and Ministry of Education, Co-Innovation Center of Neuroregeneration, Nantong University, 19 Qixiu Road, Nantong, Jiangsu 226001, China

[2]School of Life Sciences, Nantong University, 9 Seyuan Road, Nantong 226019, China

[3]School of Pharmacy, Nantong University, 19 Qixiu Road, Nantong 226001, China

[4]These authors contributed equally

[5]Lead contact

*Correspondence: lianziadd9@163.com (B.L.), lyyy111@sina.com (Y.L.), suncheng1975@ntu.edu.cn (C.S.)

https://doi.org/10.1016/j.isci.2021.102302

This is an open access article under the CC BY-NC-ND license (http://creativecommons.org/licenses/by-nc-nd/4.0/).

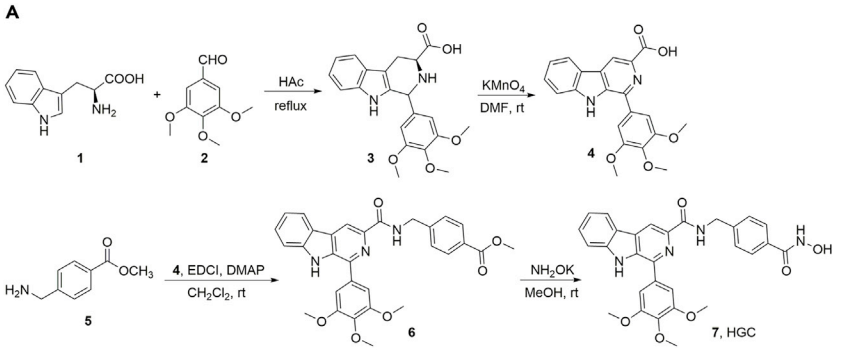

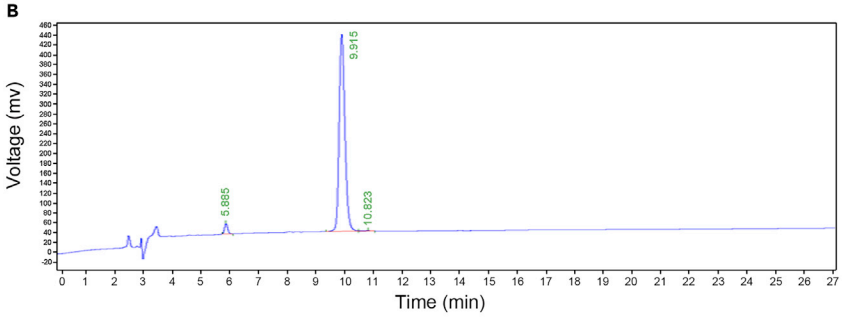

C

Compound	IC50 (nM)				
	HDAC1	HDAC2	HDAC4	HDAC6	HDAC8
HGC	8.7±0.7	> 1000	> 1000	3.8±0.5	558.7±44.6
SAHA	97.6±11.2	568.4±48.5	> 1000	48.7±5.4	174.5±14.3

Figure 1. Synthesis of HGC and HDAC inhibition activity assay

(A) Procedures for preparation of HGC.

(B) The purity of HGC was analyzed by HPLC.

(C) HDAC inhibition activity tests. HDAC activity was assayed by using recombinant HDACs and their substrates. The detailed procedures were described in transparent methods. Error bars are ±standard error of mean.

which results in a more condensed chromatin state and transcriptional repression (Narlikar et al., 2002). At this regard, by acting as epigenetic regulators, HDAC inhibitors improve histone acetylation to favor gene expression, many of which will be essential for neuronal survival (Jin et al., 2014; Sharma et al., 2019). Therefore, HDAC inhibitors have great potential capacities against PD by improving neuronal survival, especially dopaminergic neurons (Hegarty et al., 2016; Sharma et al., 2019). Indeed, recent evidence has shown that several kinds of HDAC inhibitors play beneficial roles for alleviating PD symptoms (Choong et al., 2016; Di Fruscia et al., 2015; Harrison et al., 2015; Pinho et al., 2016; Sharma et al., 2015; Suo et al., 2015).

In the present study, we synthesized an HDAC inhibitor, N-(4-(hydroxycarbamoyl)benzyl)-1-(3,4,5-trimethoxyphenyl)-9H-pyrido[3,4-b]indole-3-carboxamide (HGC), and examined its potential roles for dealing with PD both *in vitro* and *in vivo*. Our results showed that HGC protects dopaminergic neurons from 1-methyl-4-phenylpyridinium (MPP^+)-induced insults and thus ameliorates PD symptoms. Moreover, we found that these beneficial roles of HGC are dependent upon acetylation modification of NDUFV1, an enzyme in the electron transport chain (ETC) complex I.

RESULTS

HGC synthesis and HDAC inhibition activity assays

As shown in Figure 1A, N-(4-(hydroxycarbamoyl)benzyl)-1-(3,4,5-trimethoxyphenyl)-9H-pyrido[3,4-b]indole-3-carboxamide (**7**, **HGC**) was synthesized. Briefly, **5** (0.20 g, 1.2 mmol) was added to a solution of **4** (0.45 g, 1.2 mmol), 1-ethyl-3-(3-dimethylaminopropyl)carbodiimide hydrochloride (EDCI) (0.27 g, 1.44 mmol) and 4-dimethylaminopyridine (DMAP) (17 mg, 0.14 mmol) in 10 mL anhydrous CH_2Cl_2, was

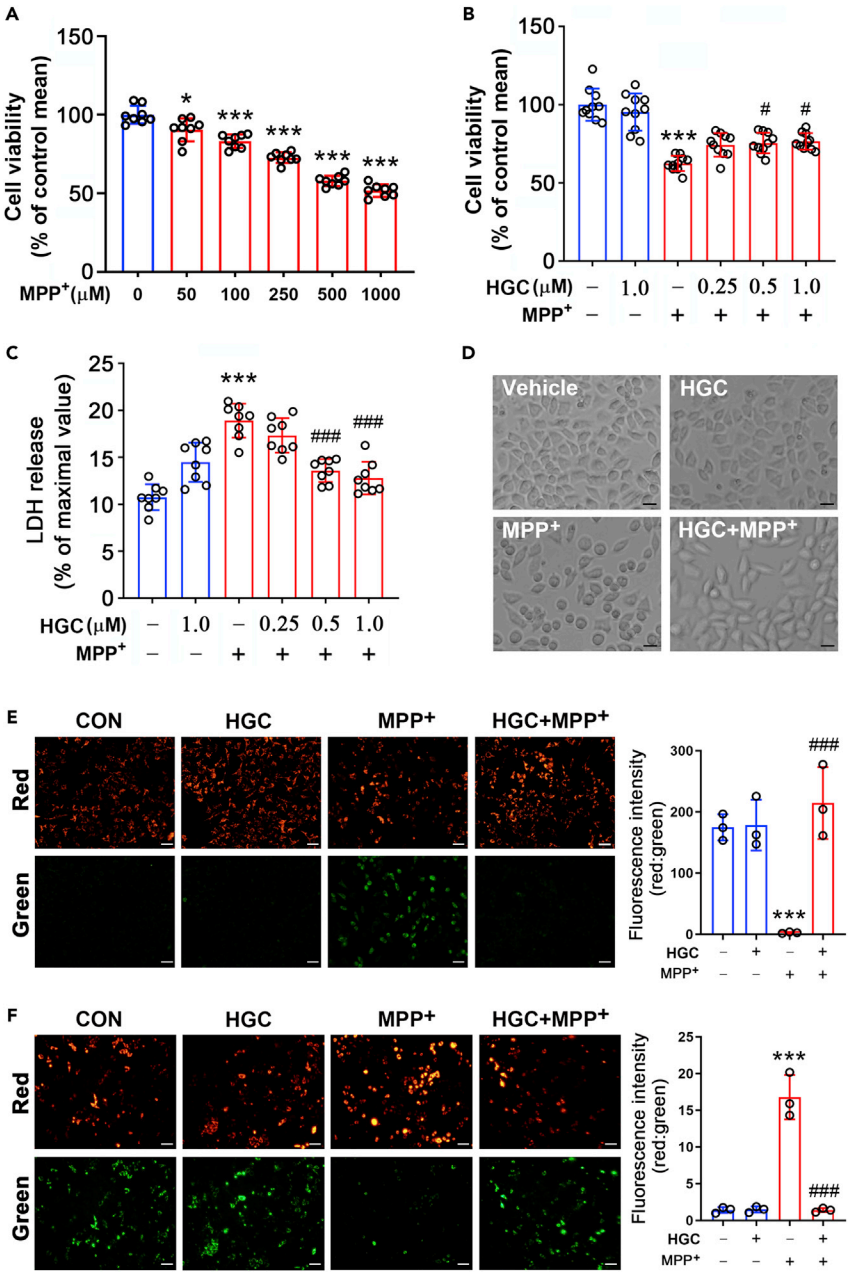

Figure 2. HGC improves cell viability of SH-SY5Y cells

(A) Effects of MPP^+ at different concentrations on cell viability. SH-SY5Y cells were treated with MPP^+ at different concentrations as indicated for 24 hr. Cell viability was assayed by MTT.

(B) MTT assay showing the increase in cell viability induced by HGC. SH-SY5Y cells were pretreated with HGC at different concentrations as indicated for 6 hr. Then, cells were subject to 500 μM of MPP^+ for additional 24 hr.

(C) The LDH release was attenuated by HGC in the MPP^+-injured cells. Cell treatments were described in (B).

(D) Cell morphology showing the protective roles of HGC in the MPP^+-treated cells. SH-SY5Y cells were pre-treated with 0.5 μM of HGC for 12 hr, and then, cells were exposed to 500 μM of MPP^+ for additional 24 hr. Cell images were taken with a microscope. Scale bar, 50 μm.

(E) JC-1 staining showing the mitochondrial membrane potential was improved by HGC. Cell treatments were described in (D). Scale bar, 50 μm.

(F) HGC decreases oxidative stress in the mitochondria. Cells were transfected with the plasmid of pMito Timer. Twelve hours after transfection, cells were treated with HGC and MPP^+ as described in (D). Scale bar, 50 μm.

Figure 2. *Continued*

Fluorescence intensity was quantified by using ImageJ software. Error bars are ±standard error of mean. *p < 0.05, ***p < 0.001 vs the control cells. #p < 0.05, ###p < 0.001 vs the cells treated with MPP^+ alone. Statistical significance was tested by two-tailed unpaired Student's *t*-test (A) or two-tailed one-way analysis of variance test (B, C, E, F).

added **5** (0.20 g, 1.2 mmol). The mixture was stirred at room temperature overnight. Then, 20 mL of CH_2Cl_2 was added, and the mixture was washed with water (30 mL × 3) and brine. The organic phase was dried over anhydrous sodium sulfate, filtered, and evaporated *in vacuo*, and the crude product was purified by column chromatography to give **6**. Intermediate **6** was then dissolved in 3 mL anhydrous methanol and poured into a solution of NH_2OK (0.09 g, 4 mmol) in 3 mL of anhydrous methanol. The mixture was stirred for 10-15 hr, and the solvent was evaporated *in vacuo*. The residue was diluted with saturated NH_4Cl aqueous solution and then extracted with ethyl acetate (6 mL × 5). The organic layers were combined, dried over anhydrous Na_2SO_4, and evaporated. The resulting residue was purified by column chromatography (eluting with ethyl acetate (EA) followed by 20:1 $CHCl_3$/MeOH followed by 10:1 $CHCl_3$/MeOH) on silica gel to afford **7** as a pale-yellow solid with a yield of 63%. Purity = 98.6% by high performance liquid chromatography (HPLC). Analytical data from nuclear magnetic resonance for **7**: MS (ESI) $m/z = 527\ [M + H]^+$; ^1H NMR (DMSO-d_6, 400 MHz): δ 11.88 (s, 1H, NH), 11.17 (s, 1H, NH), 9.34 (m, 1H, Ar-H), 8.99 (s, 1H, NH), 8.85 (s, 1H, Ar-H), 8.43 (m, 1H, Ar-H), 7.67–7.73 (m, 3H, Ar-H), 7.45 (d, 2H, $J = 8.0$ Hz, Ar-H), 7.30–7.34 (m, 3H, Ar-H), 4.66 (d, 2H, $J = 6.4$ Hz, NCH_2), 3.96 (s, 6H, OCH_3) 3.79 (s, 3H, OCH_3); HRMS (ESI): m/z calcd for $C_{29}H_{27}N_4O_6$: 526.1931; found: 527.1942 $[M + H]^+$. The purity of HGC was assayed by HPLC. Its retention time is around 9.9 min and the purity amounts to 96.8% (Figure 1B). Furthermore, we analyzed its HDAC inhibition activity, and our results showed that, as compared with suberoylanilide hydroxamic acid (SAHA), HGC exhibited more potent activity for HDAC1 and HDAC6 (Figure 1C).

HGC improves cell viability in SH-SY5Y cells

To investigate whether HGC has protective roles in dopaminergic neurons, SH-SY5Y cells were pre-treated with HGC and then subjected to neurotoxin MPP^+. According to the 3-(4,5)-dimethylthiahiazo (-z-y1)-3,5-diphenytetrazoliumromide (MTT) assay results, the exposure to MPP^+ greatly impaired cell viability, whereas HGC treatment increased the cell viability (Figure 2A and 2B). Furthermore, we also analyzed lactate dehydrogenase (LDH) release to ascertain the observed protective roles of HGC against MPP^+ injury. As shown in Figure 2C, the LDH release was markedly increased in the presence of MPP^+. As expected, the treatment of HGC reduced the LDH release induced by MPP^+. The cell morphology showed that MPP^+ insult largely decreases cell viability as evidenced by shrunk cell shapes (Figure 2D). The pretreatment of HGC greatly prevented this decline. MPP^+ is a potent neurotoxin, which can induce mitochondrial dysfunction. Therefore, we analyzed mitochondrial function in the following experiments. First, JC-1 staining was employed to evaluate mitochondrial membrane potential (MMP). JC-1 dye exhibits potential-dependent accumulation in mitochondria, indicated by a green fluorescence for the monomeric form of the probe, which shifts to red with a concentration-dependent formation of red fluorescence J-aggregates (Reers et al., 1991). Consequently, mitochondrial depolarization is indicated by a decrease in the red/green fluorescence intensity ratio. The results showed that the MMP was dramatically reduced by MPP^+; and the presence of HGC almost completely restored the MMP in SH-SY5Y cells (Figure 2E). Next, we transfected the cells with the plasmid of pMito Timer to detect oxidative stress in mitochondria (Laker et al., 2014). *MitoTimer* encodes a mitochondria-targeted green fluorescent protein when newly synthesized, which shifts irreversibly to red fluorescence when oxidized. The results showed that MPP^+ induced a remarkable fluorescence shift toward red, indicating enhanced oxidative stress in mitochondria. HGC treatment resulted in a significant fluorescence shift toward green (Figure 2F). The above data clearly show that HGC, a newly synthesized histone deacetylase inhibitor, protects SH-SY5Y cells from MPP^+-induced insults.

HGC improves cell viability in primary dopaminergic neurons

Next, we sought to recapitulate the observed protective roles of HGC in rat primary dopaminergic neurons (Figure S1). The cell viability in primary dopaminergic neurons was gradually reduced by the increasing concentrations of MPP^+ (Figure 3A). As well as in SH-SY5Y cells, the presence of HGC improved cell viability and reduced LDH activity in primary dopaminergic neurons treated with MPP^+ (Figures 3B and 3C). Cell morphology further confirmed the protective roles of HGC (Figure 3D). The MMP was decreased markedly in MPP^+-treated primary dopaminergic neurons, whereas HGC treatment partially recovered the MMP (Figure 3E). These data further confirm the protective roles of HGC in dopaminergic neurons.

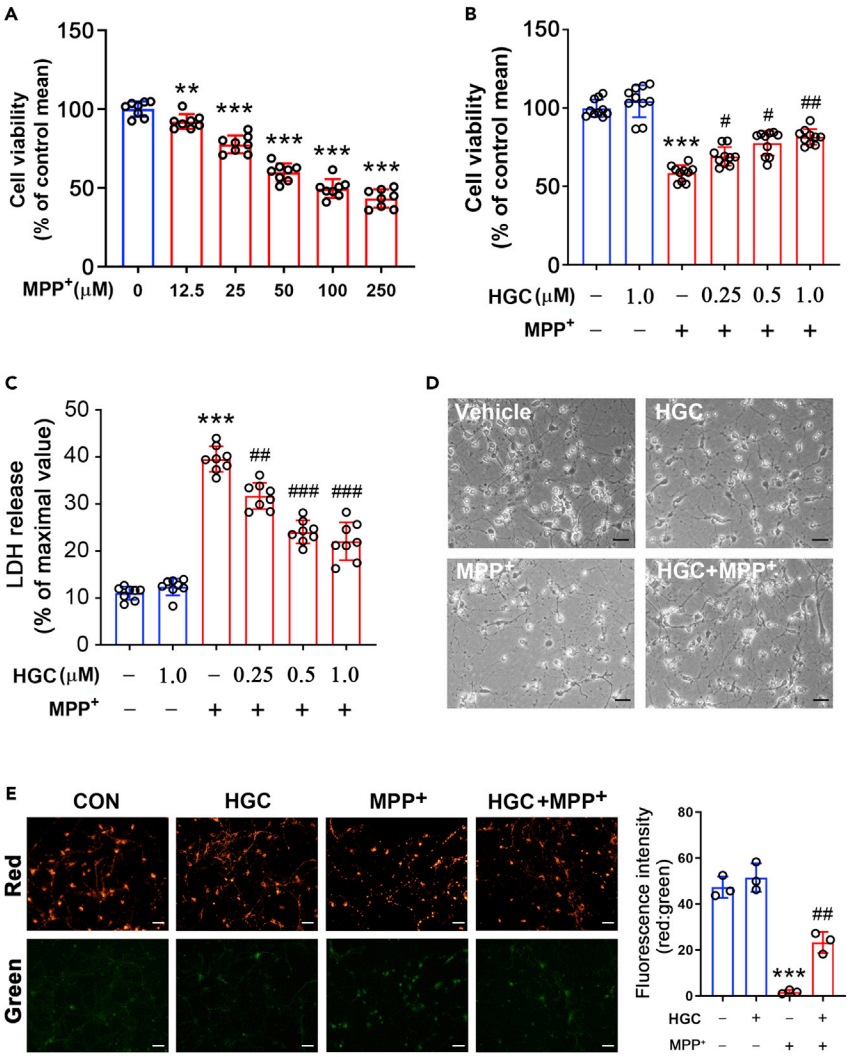

Figure 3. HGC improves cell viability of primary dopaminergic neurons

(A) Effects of MPP^+ at different concentrations on cell viability. Primary dopaminergic neurons were treated with MPP^+ at different concentrations as indicated for 24 hr. Cell viability was assayed by MTT.

(B) MTT assay showing the cell viability was improved by HGC. Primary dopaminergic neurons were pretreated with HGC at different concentrations as indicated for 6 hr. Then, neurons were subjected to 50 μM of MPP^+ for additional 24 hr.

(C) The LDH release was decreased by HGC. Cell treatments were described in (B).

(D) Cell morphology. Primary dopaminergic neurons were pre-treated with 0.5 μM of HGC for 12 hr, and then, neurons were exposed to 50 μM of MPP^+ for additional 24 hr. Cell images were taken with a microscope. Scale bar, 50 μm.

(E) JC-1 staining showing the mitochondrial membrane potential was improved by HGC. Cell treatments were described in (D). Scale bar, 50 μm.

Error bars are ±standard error of mean. ***$p < 0.001$ vs the control cells. #$p < 0.05$, ##$p < 0.01$, and ###$p < 0.001$ vs the cells treated with MPP^+ alone. Statistical significance was tested by two-tailed unpaired Student's *t*-test (A) or two-tailed one-way analysis of variance test (B, C, E).

HGC rectifies behavioral defects in PD model mice

The observed neuroprotective roles of HGC prompt us to examine its therapeutic potentials for dealing with dopaminergic neuron loss-associated diseases such as PD. Thus, 1-methyl-4-phenyl-1, 2, 3, 6-tetra-hydropyridine (MPTP)-induced PD model mice were employed for this aim. The whole experimental scheme is illustrated in Figure 4A. Motor dysfunction is a main characteristic of PD, and therefore, we analyzed behavioral performances. The results showed that MPTP treatment induced behavioral defects in rotarod, pole, and traction tests (Figures 4B–4D). As expected, HGC intervention largely rectified these behavioral defects (Figures 4B–4D). Moreover, olfactory tests revealed that HGC treatment shortened

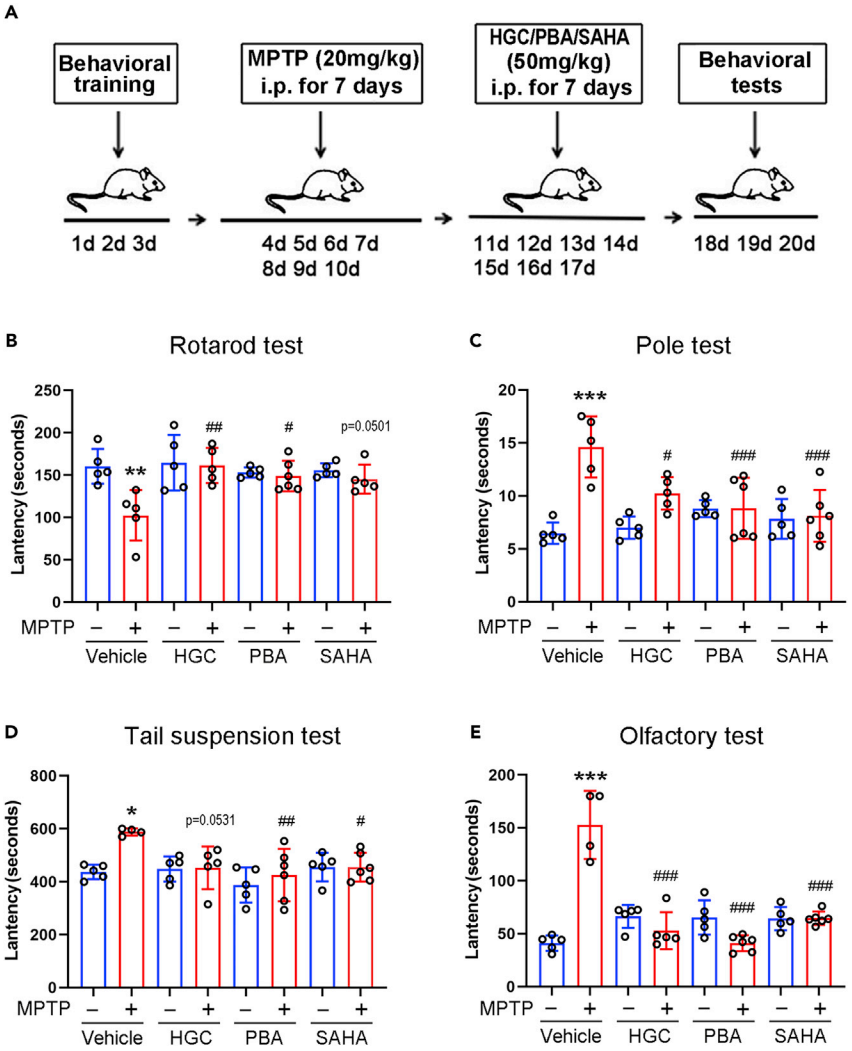

Figure 4. HGC improves behavioral performance in Parkinson model mice

(A) Timeline of the experiments.

(B) Rotarod test.

(C) Pole test.

(D) Tail suspension test.

(E) Olfactory test.

Error bars are ±standard error of mean. n = 5. *p < 0.05, **p < 0.01, and ***p < 0.001 versus the control mice in the vehicle group. #p < 0.05, ##p < 0.01, and ###p < 0.001 versus the mice treated with MPTP in the vehicle group. Statistical significance was tested by two-tailed unpaired Student's *t*-test.

the time to find hidden food (Figure 4E). Meanwhile, we also compared the anti-PD roles of HGC with other two well-known HDAC inhibitors, SAHA and phenylbutyrate (PBA). As well as HGC, both SAHA and PBA exhibited beneficial roles against PD as evidenced by improved behavioral performances (Figures 4B–4E). The anti-PD roles of these chemicals are comparable at the dosage of 50 mg/kg/day for 7 days; however, due to high molecular weight of HGC (HGC: 526.19; SAHA: 264.32; PBA: 186.18), we speculate that HGC may have better efficacy for treating PD. These results clearly indicate that HGC plays a beneficial role for dealing with motor dysfunctions in PD mice.

HGC prevents TH loss in the SNpc in PD model mice

Dopaminergic neurons loss in the SNpc is closely related with PD progression. Hence, we next analyzed dopaminergic neurons in the SNpc. First, we analyzed the total neurons in the midbrain by Nissl staining.

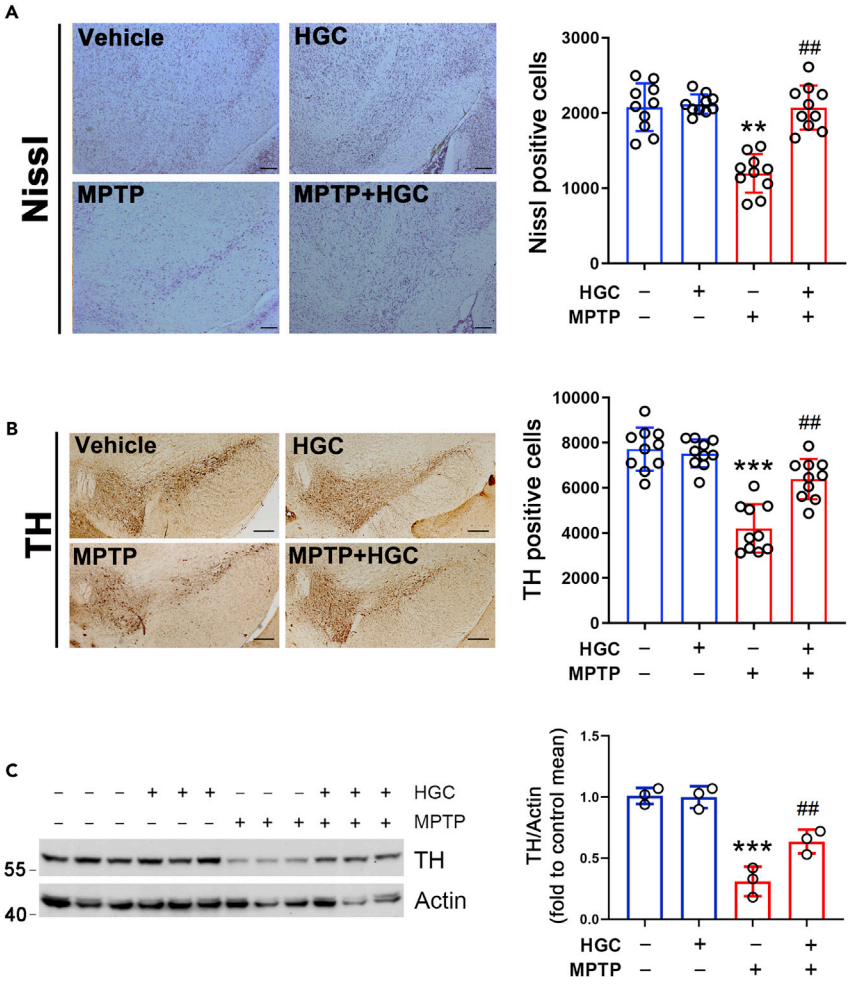

Figure 5. HGC prevents TH loss in the SNpc in PD model mice

(A) Nissl staining. Scale bar, 200 μm.

(B) Immunochemical analysis of TH expression in the SNpc. Scale bar, 200 μm.

(C) Western blot analysis of the protein levels of TH in the SNpc. Actin was used as a loading control.

Error bars are ±standard error of mean. n = 5. **p < 0.01, ***p < 0.001 vs the vehicle-treated mice. ##p < 0.01 vs the mice treated with MPTP alone. Statistical significance was tested two-tailed one-way analysis of variance test.

The results showed that MPTP treatment induced a reduction in total neurons and HGC prevented this trend (Figure 5A). Following immunohistochemical data showed that tyrosine hydroxylase (TH)-positive neurons were dramatically decreased in the SNpc in PD model mice and HGC treatment counteracted this decline (Figure 5B). Furthermore, Western blot data also showed similar changes in TH expression, i.e., HGC prevented the reductions in TH expression in the SNpc induced by MPTP (Figure 5C). Additionally, we also examined TH expression in the striatum. Both immunohistochemical and Western blot data showed that TH expression in the striatum was decreased by MPTP, while HGC treatment largely prevented this decrease (Figures 6A and 6B). These data indicate that HGC prevents TH-positive neuron loss in PD model mice.

HGC improves mitochondrial integrity in PD models

Our above results showed that HGC improves mitochondrial functions in dopaminergic neurons treated with MPP^+. To further confirm this notion, we analyzed ultra-structure of mitochondria by using electron microscopy. As shown in Figure 7A, the mitochondrial integrity was destroyed, and the cristae were smeared in SH-SY5Y cells treated with MPP^+. These defects in mitochondrial structures were ameliorated in the presence of HGC. In the midbrain of mice, the mitochondria showed elaborate and compactly

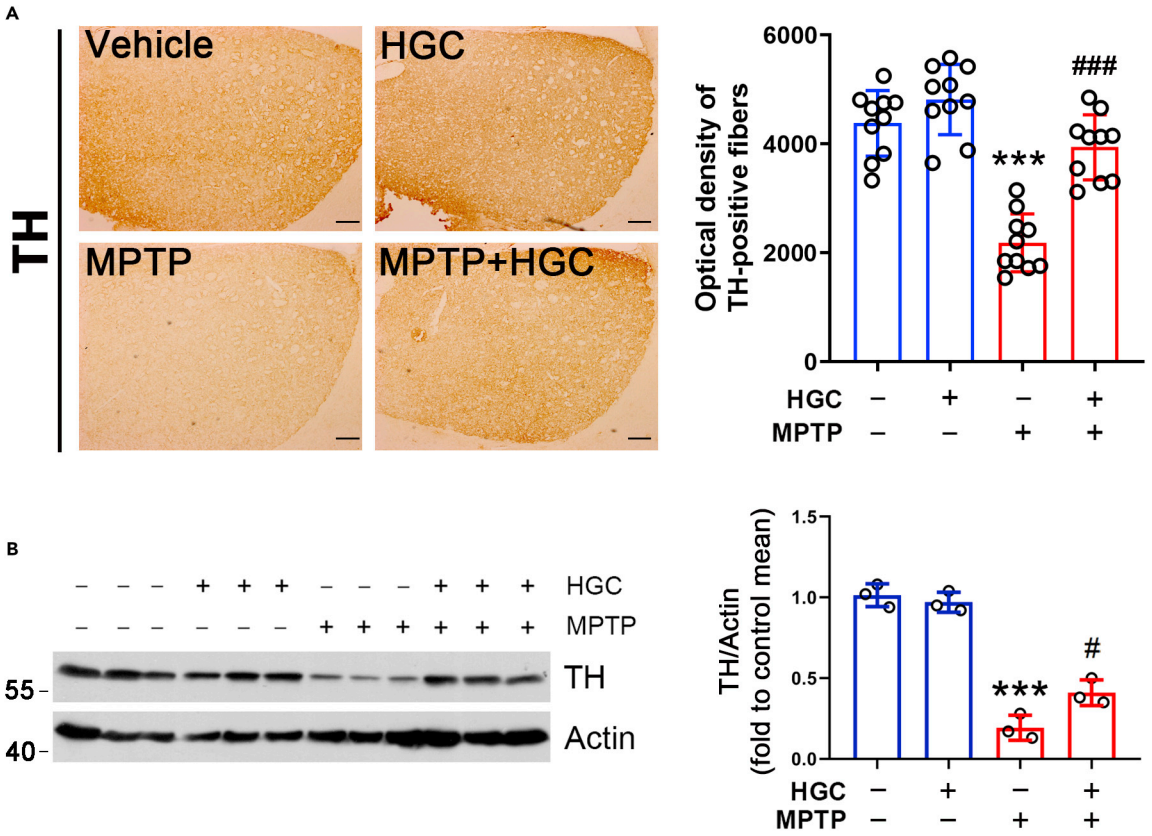

Figure 6. HGC prevents TH loss in the striatum in PD model mice

(A) Immunochemical analysis of TH expression in the striatum. Relative density of TH-positive neuronal fibers in the striatum was quantified. Scale bar, 200 μm.

(B) Western blot analysis of the protein levels of TH in the striatum. Actin was used as a loading control. Error bars are ±standard error of mean. n = 5. ***$p < 0.001$ vs the vehicle-treated mice. #$p < 0.05$, ###$p < 0.001$ vs the mice treated with MPTP alone. Statistical significance was tested by two-tailed one-way analysis of variance test.

packed cristae in the mice treated with vehicle or HGC (Figure 7B). In MPTP-treated mice, the cristae structures in the mitochondria were severely destroyed; however, the application of HGC improved the mitochondrial structures in mice treated with MPTP (Figure 7B). Accordingly, the mitochondrial DNA copy number was decreased by MPTP, and HGC prevented this decline (Figure 7C). In line with increased mitochondrial content, HGC treatment enhanced the expression of enzymes involved in oxidative phosphorylation, including PHB1, VDHC, SDHA, Cox IV, and HSP60 (Figures 7D and 7E). These data further confirm that HGC improves mitochondrial structures and functions in MPP^+-induced PD models.

HGC induces acetylation in NDUFV1 at lysine 28

The above data showed that HGC plays beneficial roles for protecting dopaminergic neurons from MPP^+-induced insults. In the following experiments, we tried to reveal the underlying molecular mechanisms. To this aim, we treated SH-SY5Y cells with HGC and prepared the total protein lysates for mass spectrometry analysis. Since HGC is an inhibitor of HDACs, we focused our interest on acetylation modification. The mass data indicated that 91 proteins were acetylated at lysine residues (Table S1. Mass spectrometry data. Related to Figure 8.). Of these, one protein named as NDUFV1 got our attention due to its critical roles in mitochondrial functions. The mass results showed that lysine 28 in NDUFV1 was acetylated in cells treated with HGC (Figure 8A). This residue was conserved across several species (Figure 8B). To further confirm the acetylation site in NDUFV1, we treated SH-SY5Y cells with HGC and performed immunoprecipitation and the resulting immuno-complex was subjected to Western blot analysis. Indeed, acetylated NDUFV1 was increased by HGC in a dose-dependent manner (Figure 8C). Furthermore, we constructed a mutated form of NDUFV1 in which lysine 28 was mutated into arginine

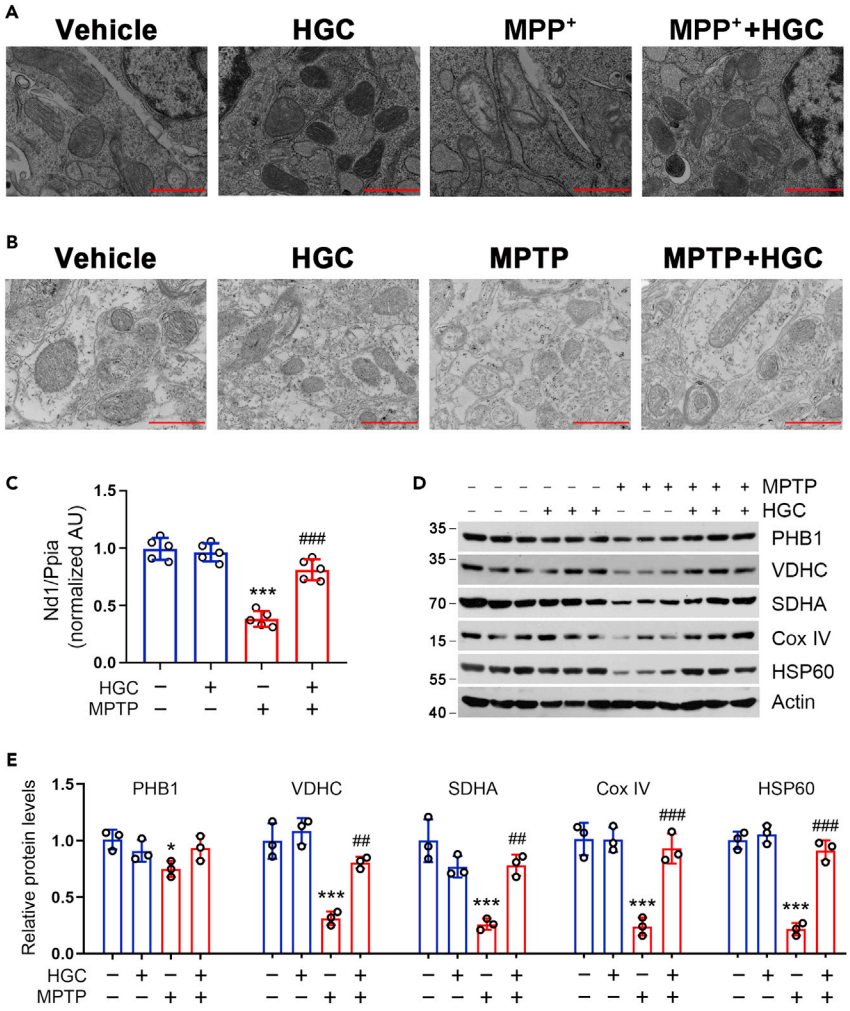

Figure 7. HGC improves mitochondrial function in PD model cells and mice

(A) HGC maintains mitochondria morphology in SH-SY5Y cells. SH-SY5Y cells were pre-treated with 0.5 μM of HGC for 12 hr, and then, cells were exposed to 500 μM of MPP^+ for additional 24 hr. Mitochondria images were monitored with an electron microscope. Scale bar, 1 μm.

(B) HGC improves mitochondrial integrity in the SNpc. PD model mice induced by MPTP were injected with HGC at the dosage of 50 mg/kg/day for consecutive 7 days. Mitochondria images were monitored with an electron microscope. Scale bar, 1 μm.

(C) HGC enhanced mitochondrial DNA copy number in the midbrain of mice treated with MPTP. Mitochondrial DNA quantification was evaluated by Nd1/Ppia (*Nd1* is a mitochondrial gene and *Ppia* is a nuclear gene).

(D) Analysis of electron transport chain protein expression. Samples were prepared from the midbrain, and protein levels were analyzed by Western blot. Actin was used as a loading control.

(E) Quantification analysis for Western blot data as shown in (D).

Error bars are ±standard error of mean. n = 5. *$p < 0.05$, ***$p < 0.001$ vs the vehicle-treated mice. ##$p < 0.01$, ###$p < 0.001$ vs the mice treated with MPTP alone. Statistical significance was tested by two-tailed one-way analysis of variance test.

(K28A). Unlike wild-type NDUFV1, which was acetylated in the presence of HGC, NDUFV1 K28A was not acetylated by HGC (Figure 8D). MPP^+ treatment induced a decrease in acetylated NDUFV1, while HGC could prevent this trend (Figure 8E). These results indicate that HGC stimulates acetylation modification of NDUFV1 at lysine 28, implying NDUFV1 might be a target of HGC for mediating its neuroprotective roles.

HGC-induced acetylation of NDUFV1 at lysine 28 is mediated by HDAC6

Next, we planned to explore which HDAC mediates the acetylation modification of NDUFV1 at lysine 28 induced by HGC. Therefore, co-immunoprecipitation was employed for analyzing the potential HDAC(s).

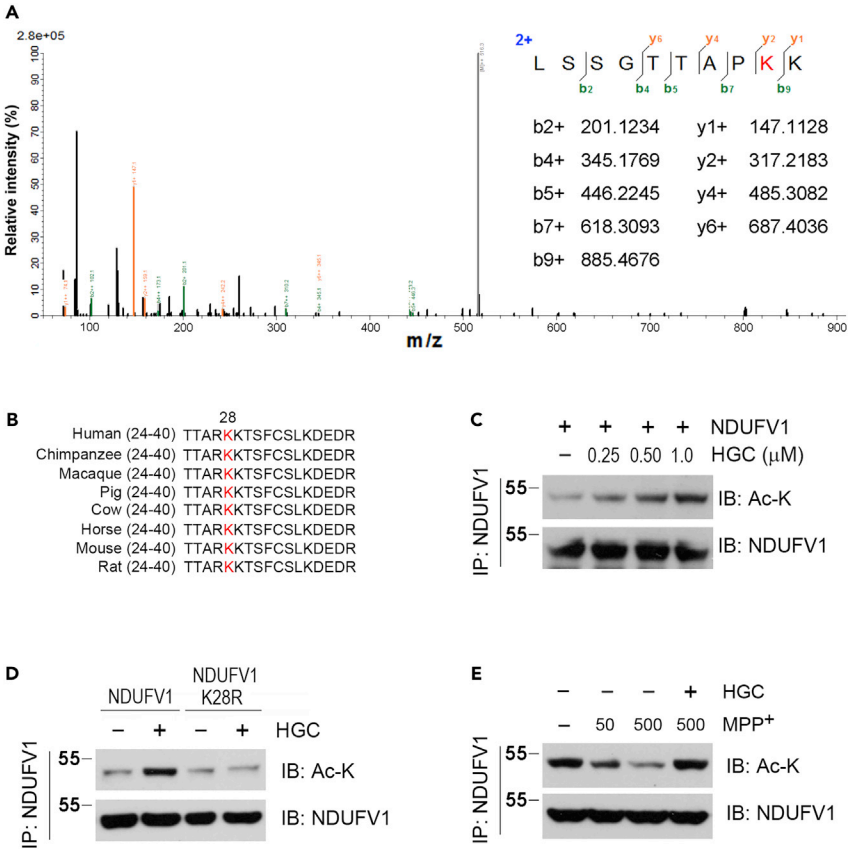

Figure 8. HGC stimulates NDUFV1 acetylation at K28

(A) Identification of acetylation site in NDUFV1 by tandem mass spectrometry. SH-SY5Y cells were treated with 1.0 μM of HGC for 24 hr. Total protein lysates were prepared for mass spectrometry analysis.

(B) Sequence alignment of the putative acetylation site of K28 in NDUFV1 from different species.

(C) HGC increases acetylated NDUFV1. SH-SY5Y cells were transfected with the plasmid expressing NDUFV1. Twelve hours after transfection, cells were incubated with HGC (0.25, 0.50, or 1.0 μM) for additional 24 hr. Total cell lysates were subjected to immunoprecipitation and Western blot analysis.

(D) HGC has no effect on acetylated NDUFV1 in mutated NDUFV1 (NDUFV1 K28R). SH-SY5Y cells were transfected with wild-type NDUFV1 or mutated NDUFV1. Twelve hours after transfection, cells were treated with 1.0 μM of HGC as indicated for additional 24 hr. Total cell lysates were prepared for immunoprecipitation using anti-NDUFV1, and immuno-complex was analyzed by Western blot.

(E) HGC prevents the decreased acetylated NDUFV1 in the cells treated with MPP^+. SH-SY5Y cells were treated with 500 μM of MPP^+ and 1.0 μM of HGC as indicated for 24 hr. Total protein lysates were prepared and subjected to immunoprecipitation using anti-NDUFV1 antibody. The resulting immuno-complex was analyzed by Western blot.

Ac-K, acetylated lysine; IP, immunoprecipitation; IB, immunoblot.

NDUFV1 is a nuclear gene coding protein, which should be synthesized in the cytoplasm and then translocated into mitochondria. Therefore, several cytoplasmic HDACs including HDAC4, 5, 6, 7, 9, and 10 were selected for immunoblot assays. As shown in Figure 9A, HDAC4 and HDAC6 were detected in the immuno-complex, indicating these two HDACs are likely to mediate the acetylation modification of NDUFV1 at lysine 28 induced by HGC. To test which HDAC is responsible for this function, we performed immunoprecipitation experiments using anti-NDUFV1 antibody. As expected, Ac-K was increased by HGC in the immuno-complex. HDAC4 had no effect on HGC-induced Ac-K (Figure 9B). Unlike HDAC4, HDAC6 largely diminished the increased acetylated NDUFV1 induced by HGC, whereas deacetylase-deficient HDAC6 (HDAC6-DC) had no such an effect (Figure 9C). Furthermore, increased expression of HDAC6 almost completely abolished the protective roles of HGC in MPP^+-treated SH-SY5Y cells (Figure 9D). Meanwhile, HDAC4 had no effect on cell viability induced by HGC (Figure 9E). Taken together, these data indicate that HDAC6 deacetylates NDUFV1 at lysine 28; and in the presence of HGC, HDAC6 activity is inhibited, which eventually results in enhanced acetylated NDUFV1.

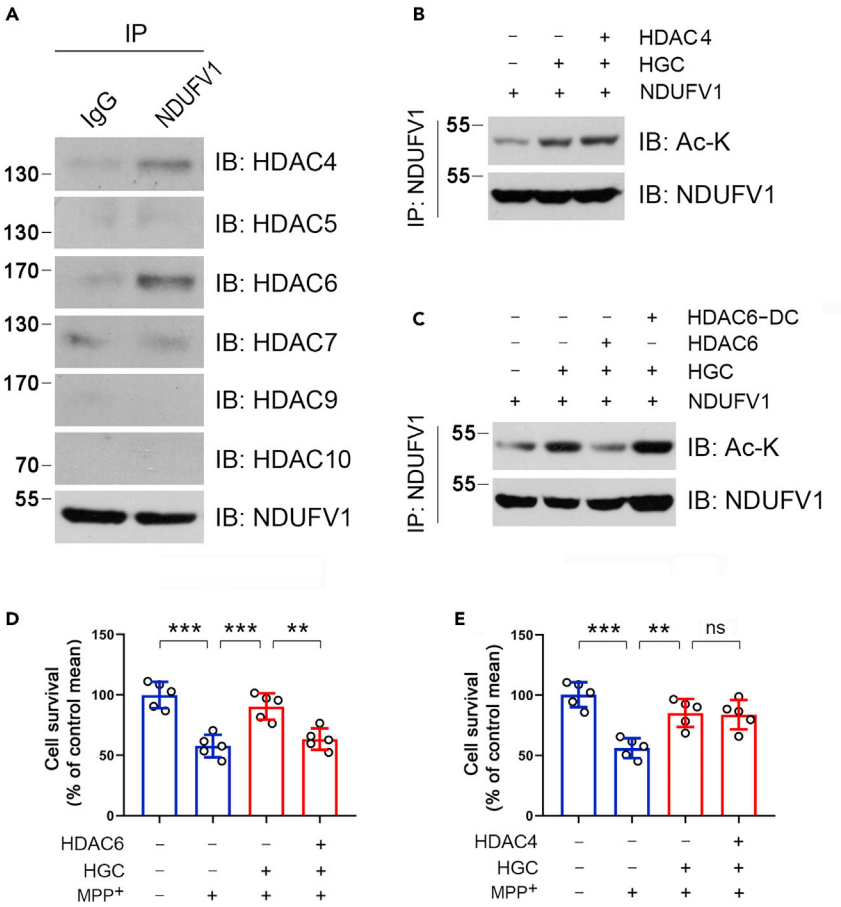

Figure 9. HDAC6 is responsible for HGC-induced acetylation of NDUFV1 at K28

(A) Co-immunoprecipitation analysis. SH-SY5Y cells were transfected with a plasmid expressing NDUFV1. Twenty-four hours after transfection, cells were harvested and subjected to co-immunoprecipitation by using an anti-NDUFV1 antibody. The resulting immune complex was analyzed by Western blot. IgG was used as a negative control.

(B) HDAC4 is not required for HGC-induced acetylation of NDUFV1. SH-SY5Y cells were transfected with plasmids expressing HDAC4 or NDUFV1 as indicated. Twelve hours after transfection, cells were incubated with or without 1.0 μM of HGC as indicated for additional 12 hr. Cells were harvested for immunoprecipitation by using an anti-NDUFV1 antibody, and the immune complex was analyzed by Western blot.

(C) Inhibition of HDAC6 by HGC increases acetylated NDUFV1. SH-SY5Y cells were transfected with plasmids expressing HDAC6, HDAC6-DC, or NDUFV1 as indicated. Twelve hours after transfection, cells were incubated with or without 1.0 μM of HGC for additional 12 hr. Cells were harvested for immunoprecipitation by using an anti-NDUFV1 antibody, and the immune complex was analyzed by Western blot.

(D) Over-expression of HDAC6 mitigates enhanced cell viability induced by HGC. SH-SY5Y cells were transfected with a plasmid expressing HDAC6. Twelve hours after transfection, cells were incubated with 500 μM of MPP^+ and 1.0 μM of HGC as indicated for 24 hr. Cell viability was analyzed by the method of MTT.

(E) HDAC4 has no effect on cell viability induced by HGC. The treatments were similar to the procedures as described in (D) except HDAC4 was instead of HDAC6. IP, immunoprecipitation; IB, immunoblot; HDAC6-DC, HDAC6 deacetylase-deficient. Error bars are ±standard error of mean. $^{**}p < 0.01$ and $^{***}p < 0.001$. ns means no significance. Statistical significance was tested by two-tailed one-way analysis of variance test.

HGC improves cell viability by stimulating NDUFV1 acetylation in SH-SY5Y cells

To test whether NDUFV1 is a target for mediating neuroprotective roles of HGC, we first examined the potential roles of NDUFV1 on cell viability. To test this hypothesis, we increased NDUFV1 in SH-SY5Y cells by transfection with the plasmid expressing *Ndufv1*. Our results showed that NDUFV1 was markedly increased by the transfection (Figure 10A). Cell viability assays showed that NDUFV1 increased cell viability in the cells treated with or without MPP^+ (Figure 10B). JC-1 staining showed that the MMP was decreased by MPP^+, and NDUFV1 largely counteracted this trend (Figure 10C). The increased oxidative stress in MPP^+-treated

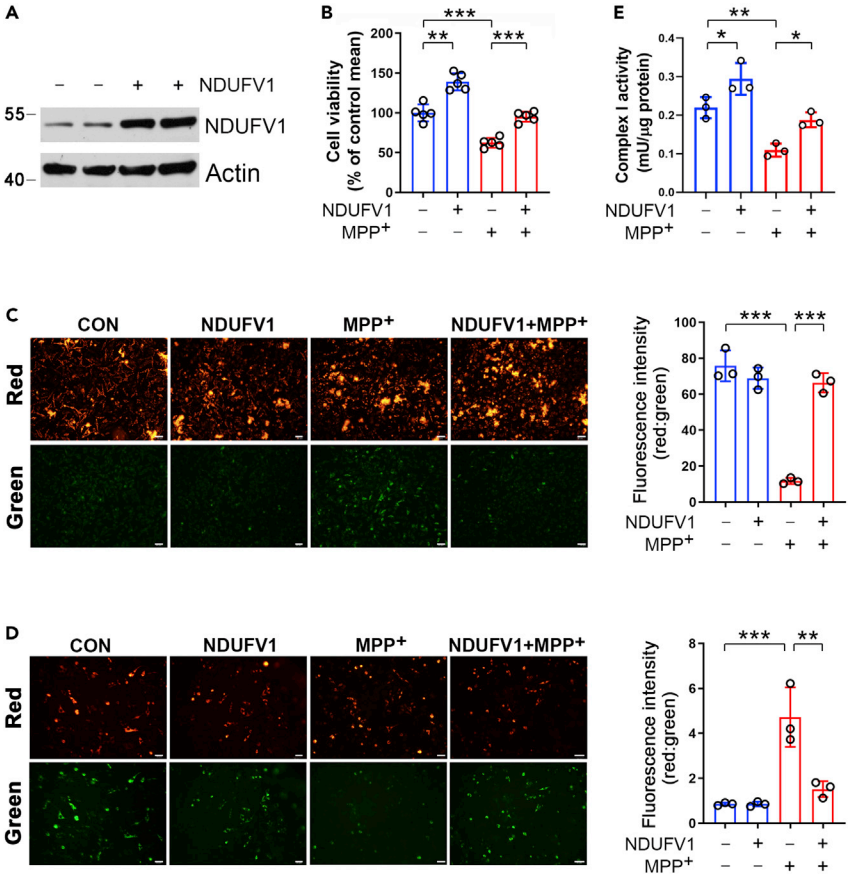

Figure 10. NDUFV1 attenuates cell injuries induced by MPP+

(A) Increased expression of NDUFV1 by the transfection. SH-SY5Y cells were transfected with the plasmid bearing *Ndufv1*. Twenty-four hours after transfection, cell lysates were prepared and subjected to Western blot analysis. Actin was used a loading control.

(B) NDUFV1 improves cell viability. SH-SY5Y cells were transfected with the plasmid expressing *Ndufv1*. Twelve hours after transfection, cells were treated with 500 μM of MPP^+ for additional 24 hr. Cell viability was assayed by the method of MTT.

(C) JC-1 staining. SH-SY5Y cells were treated as mentioned above, and mitochondrial function was analyzed by JC-1 staining. Fluorescence intensity was measured by using ImageJ software. Scale bar, 50 μm.

(D) Analysis of oxidative stress in the mitochondria. SH-SY5Y cells were co-transfected with the plasmids expressing *Ndufv1* and *pMitoTimer*. Twelve hours after transfection, cells were treated with 500 μM of MPP^+ for additional 24 hr. Oxidative stress in the mitochondria was analyzed by the shift from green color to red color with a fluorescence microscopy. Fluorescence intensity was quantified by using ImageJ software. Scale bar, 50 μm.

(E) The mitochondria complex I activity was improved by NDUFV1. SH-SY5Y cells were transfected with the plasmid expressing *Ndufv1*. Twelve hours after transfection, cells were treated with 500 μM of MPP^+ for additional 24 hr. Mitochondria were isolated and subjected to the complex I activity assay. Error bars are ±standard error of mean. *$p < 0.05$, **$p < 0.01$, and ***$p < 0.001$. Statistical significance was tested by two-tailed one-way analysis of variance test.

cells was reduced markedly by HGC (Figure 10D). Furthermore, the mitochondria complex I activity was improved by NDUFV1 (Figure 10E). These data strongly indicate that NDUFV1 has a capacity for protecting dopaminergic neurons from MPP^+-induced insults.

Next, we downregulated NDUFV1 expression by siRNAs and examined whether the observed neuroprotective roles of HGC are dependent upon NDUFV1. The results showed that NDUFV1 expression was dramatically reduced by its siRNAs; of these siRNAs, siRNA-2# exhibited the best knockdown efficiency (Figures 11A and 11B); therefore, it was chosen for the following experiments. Knockdown of NDUFV1 abolished HGC-mediated improved cell viability in cells treated with MPP^+ (Figure 11C). Mitochondrial function assays also revealed that NDUFV1 knockdown largely weakened the neuroprotective roles of HGC in

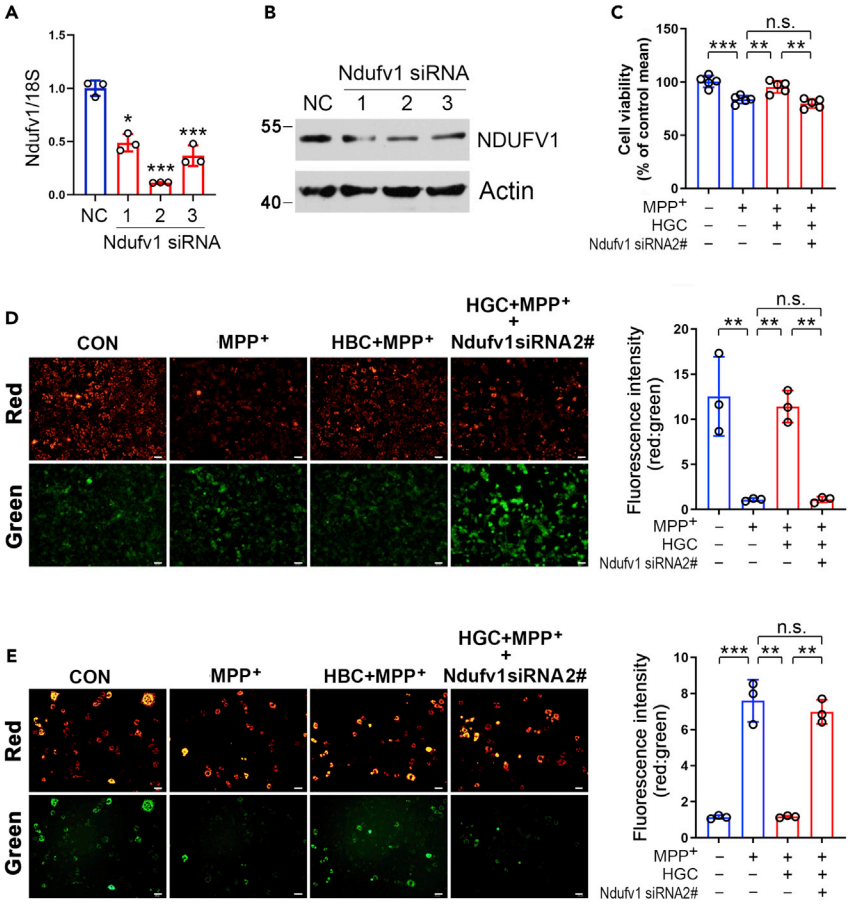

Figure 11. Knockdown of NDUFV1 abolishes the neuroprotective roles of HGC

(A) siRNAs mediated knockdown in NDUFV1. SH-SY5Y cells were transfected with siRNAs against *Ndufv1*. Seventy-two hours after transfection, cells were harvested for total RNA extraction and quantitative real-time PCR analysis. 18S was used as a house-keeping gene.

(B) Effects of siRNAs on NDUFV1 protein levels. Cell treatments were described in (A). At the end of treatments, total cell lysates were prepared for Western blot analysis. Actin was used as a loading control.

(C) NDUFV1 knockdown abolishes the improved cell viability induced by HGC. SH-SY5Y cells were transfected with *Ndufv1* siRNA-2#. Forty-eight hours after transfection, cells were treated with 1.0 μM of HGC and 500 μM MPP^+ as indicated for additional 24 hr. Cell viability was assayed by MTT.

(D) JC-1 staining. Cell treatments were described in (C). Mitochondrial function was analyzed by JC-1 staining. Fluorescence intensity was measured by using ImageJ software. Scale bar, 50 μm.

(E) Analysis of oxidative stress in the mitochondria. SH-SY5Y cells were transfected with *Ndufv1* siRNA-2#. Thirty-six hours after transfection, cells were transfected with the plasmid of *pMito Timer* for 12 hr, and then, cells were treated with 1.0 μM of HGC and 500 μM of MPP^+ as indicated for additional 24 hr. Oxidative stress in the mitochondria was analyzed by the shift from green color to red color with a fluorescence microscopy. Fluorescence intensity was measured by using ImageJ software. Scale bar, 50 μm. Error bars are ±standard error of mean. *$p < 0.05$, **$p < 0.01$, and ***$p < 0.001$. ns, no significance. Statistical significance was tested by two-tailed unpaired Student's *t*-test (A) or two-tailed one-way analysis of variance test (C–E).

MPP^+-treated cells (Figures 11D and 11E). Together, the above data clearly show that the neuroprotective roles of HGC in dopaminergic neurons are dependent upon acetylation of NDUFV1.

DISCUSSION

A growing amount of evidence indicates that HDAC inhibitors are potent candidates for developing drugs for dealing with PD (Chen et al., 2012; Choong et al., 2016; Di Fruscia et al., 2015; Harrison et al., 2015, 2019; Kidd and Schneider, 2011; Rane et al., 2012; Sharma et al., 2015). In the present study, we synthesized a

compound named as HGC and examined its anti-PD capacity both *in vitro* and *in vivo*. Our data showed that HGC protects cultured dopaminergic neurons from MPP^+-induced apoptosis. Moreover, in MPTP-induced PD model mice, HGC application shows multiple beneficial roles including rectifying behavioral defects, maintaining TH expression in the SNpc and striatum, and improving mitochondrial function. Mechanistically, NDUFV1, an enzyme belonging to complex I of the mitochondrial ETC, was found to be acetylated at lysine 28 in the presence of HGC, and HDAC6 is a mediator for this modification. Following experiments revealed that elevated expression of NDUFV1 attenuates cell injuries induced by MPP^+; on the contrary, NDUFV1 knockdown further aggravates MPP^+-induced insults. Most importantly, NDUFV1 knockdown almost completely abolishes the neuroprotective effects of HGC, indicating NDUFV1 is a target of HGC for mediating its neuroprotective roles in dopaminergic neurons.

Based on function and DNA sequence similarity, HDAC proteins are grouped into four classes, i.e., class I, II, III, and IV. Of these, class I, II, and IV are considered as classical HDACs whose activities are inhibited by trichostatin A (TSA) and have zinc-dependent active sites (Narlikar et al., 2002). Known as sirtuins, class III HDAC activities are in an NAD-dependent manner and are not affected by TSA (Narlikar et al., 2002). By deacetylating lysine residues in histone or non-histone proteins, HDAC proteins exhibit multiple fundamental roles in neurodegenerative disorders including Alzheimer disease (AD), polyglutamine disorders, and PD (Saha and Pahan, 2006; Thomas and D'Mello, 2018). In general, inhibition of HDACs elicits hyperacetylation of histone or non-histone proteins and thus shows beneficial roles against neurodegenerative disorders (Cook et al., 2014). Accordingly, the research and development of HDAC inhibitors has gained much attention and is considered as a potential therapeutic strategy for treating these diseases (Hegarty et al., 2016).

Indeed, HDAC inhibitors have been shown to be effective in numerous different mouse models of neurodegenerative diseases. As for PD, several kinds of HDAC inhibitors including sodium butyrate (SB), valproic acid (VPA), and suberoylanilide hydroxamic acid (SAHA) increase cell viability and enhance the number of TH-positive cells under MPP^+ or 6-hydrodopamine treatment (Chen et al., 2012; Kidd and Schneider, 2011; Rane et al., 2012). In line with these results, we also found that HGC, a newly synthesized inhibitor of HDACs, rectifies behavioral defects and increases TH-positive neurons in PD model mice induced by MPTP. On the contrary, a recent study has shown that nicotinamide, a potent inhibitor of HDAC class III, exacerbates neurodegeneration in the lactacystin rat model of PD (Harrison et al., 2019). In accordance, SIRT3, a member of HDAC class III, was found to be capable of increasing cell viability in cultured PD model cells (Zhang et al., 2018); and deletion of *Sirt3* promotes oxidative stress and reduces the mitochondrial function in dopaminergic neurons (Shi et al., 2017). Therefore, the potential roles of HDACs in neurodegenerative disorders are not consistent, i.e. they play neuroprotective or neurotoxic effects, which may dependent upon the subtypes of HDACs (Thomas and D'Mello, 2018).

With comparison to other HDAC inhibitors such as SB, VPA, and SAHA, the newly synthesized HDAC inhibitor HGC was derived from harmine. It has been shown that harmine possesses multiple neuroprotective roles including anti-inflammation, anti-oxidative stress, and stimulation brain-derived neurotrophic factor expression (Dos Santos and Hallak, 2017; Piechowska et al., 2019; Zhong et al., 2015). At this regard, therefore, HGC may hold better benefits than other HDAC inhibitors in neurodegenerative disorders. In the present study, we also compared the anti-PD effects of several HDAC inhibitors such as HGC, SAHA, and PBA. Although their efficacies are comparable at the same dosage (50 mg/kg/day), however considering their respective molecular weight (HGC, 526.19; SAHA, 264.32; PBA, 186.18), HGC has the best efficacy for dealing with PD. Another issue regarding the dosage of MPP^+ in cultured cells or neurons should be clarified. To choose an appropriate dosage of MPP^+ in *in vitro* models, a series of MPP^+ at different concentrations were used. Based upon our results, we chose 500 μM and 50 μM of MPP^+ to treat SH-SY5Y cells and primary dopaminergic neurons, respectively. In a previous report, 5 μM of MPP^+ was used to treat primary dopaminergic neurons, which is quite lower as compared with the current dosage (Collins et al., 2015). This discrepancy may result from different cell culture conditions.

HDAC6 is a cytoplasmic protein and it has two catalytic domains (Gregoretti et al., 2004). Earlier studies suggest that HDAC6 is a specific α-tubulin deacetylase (Zhang et al., 2008). Following investigations revealed that HDAC6 can deacetylate many other substrates including tau, HSP90, β-catenin, the tumor suppressor macrophage stimulating 1, cortactin, and Miro1 (Cook et al., 2014; Kalinski et al., 2019; Kekatpure et al., 2009; Li et al., 2008, 2016; Zhang et al., 2007). In the present study, we found that NDUFV1 also is a

substrate of HDAC6. NDUFV1 is an enzyme in the ETC complex I. As one of the entry enzymes of the ETC, complex I plays an essential role in cellular respiration or oxidative phosphorylation in mitochondria. It has been shown that complex I defects are presented in cells and tissues from patients with PD (Schapira et al., 1989). Since then, a growing number of evidence has been shown that mitochondrial dysfunction and cellular energy stress are key factors for PD pathology (Jansen et al., 2017; Wallace, 2005). In accordance, the improvements of mitochondrial biogenesis and energy metabolism play beneficial effects against neurodegenerative disorders (Rajman et al., 2018; Schondorf et al., 2018). In line with these findings, we observed that NDUFV1 is capable of increasing mitochondrial function and cell viability in MPP^+-treated cells. Moreover, HGC lost its neuroprotective roles in *Ndufv1* knockdown cells, indicating NDUFV1 is a target for mediating the neuroprotective effects of HGC in dopaminergic neurons. It is worthy to note that, HGC application-induced acetylation of NDUFV1 at lysine 28 is likely via HDAC6, i.e. HDAC6 deacetylates NDUFV1 at lysine 28; however, this deacetylation modification is inhibited in the presence of HGC since HGC is a potent inhibitor of HDAC6. Till now, there is no direct evidence showing NDUFV1 is correlated with pathology of PD. However, one bioinformatics analysis has shown that it might be involved in the pathogenesis of AD, another aging-related neurodegenerative disorder (Zhang et al., 2015). Furthermore, we also observed that NDUFV1 promotes proliferation of SH-SY5Y cells. All these findings suggest that HDAC6, together with NDUFV1, might be drug targets for developing agents to attenuate neurodegeneration in PD or potentially other neurodegenerative disorders with mitochondrial dysfunction. Most recently, one study has shown that inhibition of HDAC6 activity protects dopaminergic neurons from α-synuclein toxicity in rats (Francelle et al., 2020), which further supports our conclusions.

Limitations of the study

In the present study, we synthesized a compound named as HGC with great inhibition efficacies for HDACs, especially for HDAC1 and HDAC6. Following experiments revealed that HGC improves dopaminergic neuron viability and attenuates behavioral defects in PD modeled cells and animals. However, the biocompatibility and biosafety of HGC are still unclear, together with unknown pharmacokinetics, which impede its pharmaceutical applications in the future. Moreover, we also concerned that whether these observed anti-PD effects of HGC in this study could be recapitulated in humans.

Resource availability

Lead contact

Further information and requests for resources and reagents should be directed to and will be fulfilled by the lead contact, Cheng Sun (suncheng1975@ntu.edu.cn).

Materials availability

HGC generated in this study will be made available on request, but we may require a payment and/or a completed Materials Transfer Agreement if there is potential for commercial application.

Data and code availability

All raw data of Western blot were submitted to Mendeley Data https://data.mendeley.com/datasets.
Thiswork was supported by the National Key Research and Development Program of China (Grant No. 2017YFA0701304), the National Natural Science Foundation of China (Nos: 81770841; 81970747), the Key Natural Science Foundation of Jiangsu Higher Education Institutions (20KJA350002), and the/publish-confirmation/9s3jty3wxm/1.

METHODS

All methods can be found in the accompanying Transparent Methods supplemental file.

SUPPLEMENTAL INFORMATION

Supplemental information can be found online at https://doi.org/10.1016/j.isci.2021.102302.

ACKNOWLEDGMENTS

The authors acknowledge the Science Foundation for Basic Research from Nantong City (JC2020158).

AUTHOR CONTRIBUTIONS

B.L., Y.Y., Y.W., J.Z., J.D., X.L., Y.J., and B.L. performed the experiments. Y.L. synthesized HGC and conceived the idea. B.L. analyzed the data and wrote the manuscript. C.S. conceived the idea, supervised the study, and wrote the manuscript.

DECLARATION OF INTERESTS

The authors declare no competing interests. Part of data in this manuscript was used for patent application at China (202011449103.8).

Received: August 26, 2020
Revised: January 23, 2021
Accepted: March 10, 2021
Published: April 23, 2021

REFERENCES

Abeliovich, A., and Gitler, A.D. (2016). Defects in trafficking bridge Parkinson's disease pathology and genetics. Nature *539*, 207–216.

Armstrong, M.J., and Okun, M.S. (2020). Diagnosis and treatment of Parkinson disease: a review. JAMA *323*, 548–560.

Buck, K., and Ferger, B. (2010). L-DOPA-induced dyskinesia in Parkinson's disease: a drug discovery perspective. Drug Discov. Today *15*, 867–875.

Chen, S.H., Wu, H.M., Ossola, B., Schendzielorz, N., Wilson, B.C., Chu, C.H., Chen, S.L., Wang, Q., Zhang, D., Qian, L., et al. (2012). Suberoylanilide hydroxamic acid, a histone deacetylase inhibitor, protects dopaminergic neurons from neurotoxin-induced damage. Br. J. Pharmacol. *165*, 494–505.

Choong, C.J., Sasaki, T., Hayakawa, H., Yasuda, T., Baba, K., Hirata, Y., Uesato, S., and Mochizuki, H. (2016). A novel histone deacetylase 1 and 2 isoform-specific inhibitor alleviates experimental Parkinson's disease. Neurobiol. Aging *37*, 103–116.

Collins, L.M., Adriaanse, L.J., Theratile, S.D., Hegarty, S.V., Sullivan, A.M., and O'Keeffe, G.W. (2015). Class-IIa histone deacetylase inhibition promotes the growth of neural processes and protects them against neurotoxic insult. Mol. Neurobiol. *51*, 1432–1442.

Cook, C., Stankowski, J.N., Carlomagno, Y., Stetler, C., and Petrucelli, L. (2014). Acetylation: a new key to unlock tau's role in neurodegeneration. Alzheimers Res. Ther. *6*, 29.

Di Fruscia, P., Zacharioudakis, E., Liu, C., Moniot, S., Laohasinnarong, S., Khongkow, M., Harrison, I.F., Koltsida, K., Reynolds, C.R., Schmidtkunz, K., et al. (2015). The discovery of a highly selective 5,6,7,8-tetrahydrobenzo[4,5]thieno[2,3-d] pyrimidin-4(3H)-one SIRT2 inhibitor that is neuroprotective in an in vitro Parkinson's disease model. ChemMedChem *10*, 69–82.

Dos Santos, R.G., and Hallak, J.E. (2017). Effects of the natural beta-carboline alkaloid harmine, a main constituent of ayahuasca, in memory and in the Hippocampus: a systematic literature review of preclinical studies. J. Psychoactive Drugs *49*, 1–10.

Foltynie, T., and Hariz, M.I. (2010). Surgical management of Parkinson's disease. Expert Rev. Neurother. *10*, 903–914.

Francelle, L., Outeiro, T.F., and Rappold, G.A. (2020). Inhibition of HDAC6 activity protects dopaminergic neurons from alpha-synuclein toxicity. Sci. Rep. *10*, 6064.

Gregoretti, I.V., Lee, Y.M., and Goodson, H.V. (2004). Molecular evolution of the histone deacetylase family: functional implications of phylogenetic analysis. J. Mol. Biol. *338*, 17–31.

Harrison, I.F., Crum, W.R., Vernon, A.C., and Dexter, D.T. (2015). Neurorestoration induced by the HDAC inhibitor sodium valproate in the lactacystin model of Parkinson's is associated with histone acetylation and up-regulation of neurotrophic factors. Br. J. Pharmacol. *172*, 4200–4215.

Harrison, I.F., Powell, N.M., and Dexter, D.T. (2019). The histone deacetylase inhibitor nicotinamide exacerbates neurodegeneration in the lactacystin rat model of Parkinson's disease. J. Neurochem. *148*, 136–156.

Hegarty, S.V., Sullivan, A.M., and O'Keeffe, G.W. (2016). The Epigenome as a therapeutic target for Parkinson's disease. Neural Regen. Res. *11*, 1735–1738.

Jansen, I.E., Ye, H., Heetveld, S., Lechler, M.C., Michels, H., Seinstra, R.I., Lubbe, S.J., Drouet, V., Lesage, S., Majounie, E., et al. (2017). Discovery and functional prioritization of Parkinson's disease candidate genes from large-scale whole exome sequencing. Genome Biol. *18*, 22.

Jin, H., Kanthasamy, A., Harischandra, D.S., Kondru, N., Ghosh, A., Panicker, N., Anantharam, V., Rana, A., and Kanthasamy, A.G. (2014). Histone hyperacetylation up-regulates protein kinase Cdelta in dopaminergic neurons to induce cell death: relevance to epigenetic mechanisms of neurodegeneration in Parkinson disease. J. Biol. Chem. *289*, 34743–34767.

Kalia, L.V., and Lang, A.E. (2015). Parkinson's disease. Lancet *386*, 896–912.

Kalinski, A.L., Kar, A.N., Craver, J., Tosolini, A.P., Sleigh, J.N., Lee, S.J., Hawthorne, A., Brito-Vargas, P., Miller-Randolph, S., Passino, R., et al. (2019). Deacetylation of Miro1 by HDAC6 blocks mitochondrial transport and mediates axon growth inhibition. J. Cell Biol. *218*, 1871–1890.

Kekatpure, V.D., Dannenberg, A.J., and Subbaramaiah, K. (2009). HDAC6 modulates Hsp90 chaperone activity and regulates activation of aryl hydrocarbon receptor signaling. J. Biol. Chem. *284*, 7436–7445.

Kidd, S.K., and Schneider, J.S. (2011). Protective effects of valproic acid on the nigrostriatal dopamine system in a 1-methyl-4-phenyl-1,2,3,6-tetrahydropyridine mouse model of Parkinson's disease. Neuroscience *194*, 189–194.

Laker, R.C., Xu, P., Ryall, K.A., Sujkowski, A., Kenwood, B.M., Chain, K.H., Zhang, M., Royal, M.A., Hoehn, K.L., Driscoll, M., et al. (2014). A novel MitoTimer reporter gene for mitochondrial content, structure, stress, and damage in vivo. J. Biol. Chem. *289*, 12005–12015.

Li, L., Fang, R., Liu, B., Shi, H., Wang, Y., Zhang, W., Zhang, X., and Ye, L. (2016). Deacetylation of tumor-suppressor MST1 in Hippo pathway induces its degradation through HBXIP-elevated HDAC6 in promotion of breast cancer growth. Oncogene *35*, 4048–4057.

Li, Y., Zhang, X., Polakiewicz, R.D., Yao, T.P., and Comb, M.J. (2008). HDAC6 is required for epidermal growth factor-induced beta-catenin nuclear localization. J. Biol. Chem. *283*, 12686–12690.

Narlikar, G.J., Fan, H.Y., and Kingston, R.E. (2002). Cooperation between complexes that regulate chromatin structure and transcription. Cell *108*, 475–487.

Piechowska, P., Zawirska-Wojtasiak, R., and Mildner-Szkudlarz, S. (2019). Bioactive beta-carbolines in food: a review. Nutrients *11*, 814.

Pinho, B.R., Reis, S.D., Guedes-Dias, P., Leitao-Rocha, A., Quintas, C., Valentao, P., Andrade, P.B., Santos, M.M., and Oliveira, J.M. (2016). Pharmacological modulation of HDAC1 and HDAC6 in vivo in a zebrafish model: therapeutic implications for Parkinson's disease. Pharmacol. Res. *103*, 328–339.

Poewe, W., Antonini, A., Zijlmans, J.C., Burkhard, P.R., and Vingerhoets, F. (2010). Levodopa in the

treatment of Parkinson's disease: an old drug still going strong. Clin. Interv. Aging *5*, 229–238.

Rajman, L., Chwalek, K., and Sinclair, D.A. (2018). Therapeutic potential of NAD-boosting molecules: the in vivo evidence. Cell Metab. *27*, 529–547.

Rane, P., Shields, J., Heffernan, M., Guo, Y., Akbarian, S., and King, J.A. (2012). The histone deacetylase inhibitor, sodium butyrate, alleviates cognitive deficits in pre-motor stage PD. Neuropharmacology *62*, 2409–2412.

Reers, M., Smith, T.W., and Chen, L.B. (1991). J-aggregate formation of a carbocyanine as a quantitative fluorescent indicator of membrane potential. Biochemistry *30*, 4480–4486.

Saha, R.N., and Pahan, K. (2006). HATs and HDACs in neurodegeneration: a tale of disconcerted acetylation homeostasis. Cell Death Differ. *13*, 539–550.

Schapira, A.H., Cooper, J.M., Dexter, D., Jenner, P., Clark, J.B., and Marsden, C.D. (1989). Mitochondrial complex I deficiency in Parkinson's disease. Lancet *1*, 1269.

Schondorf, D.C., Ivanyuk, D., Baden, P., Sanchez-Martinez, A., De Cicco, S., Yu, C., Giunta, I., Schwarz, L.K., Di Napoli, G., Panagiotakopoulou, V., et al. (2018). The NAD+ precursor nicotinamide riboside rescues mitochondrial defects and neuronal loss in iPSC and fly models of Parkinson's disease. Cell Rep. *23*, 2976–2988.

Sharma, S., Sarathlal, K.C., and Taliyan, R. (2019). Epigenetics in neurodegenerative diseases: the role of histone deacetylases. CNS Neurol. Disord. Drug Targets *18*, 11–18.

Sharma, S., Taliyan, R., and Singh, S. (2015). Beneficial effects of sodium butyrate in 6-OHDA induced neurotoxicity and behavioral abnormalities: modulation of histone deacetylase activity. Behav. Brain Res. *291*, 306–314.

Shi, H., Deng, H.X., Gius, D., Schumacker, P.T., Surmeier, D.J., and Ma, Y.C. (2017). Sirt3 protects dopaminergic neurons from mitochondrial oxidative stress. Hum. Mol. Genet. *26*, 1915–1926.

Suo, H., Wang, P., Tong, J., Cai, L., Liu, J., Huang, D., Huang, L., Wang, Z., Huang, Y., Xu, J., et al. (2015). NRSF is an essential mediator for the neuroprotection of trichostatin A in the MPTP mouse model of Parkinson's disease. Neuropharmacology *99*, 67–78.

Thomas, E.A., and D'Mello, S.R. (2018). Complex neuroprotective and neurotoxic effects of histone deacetylases. J. Neurochem. *145*, 96–110.

Wallace, D.C. (2005). A mitochondrial paradigm of metabolic and degenerative diseases, aging, and cancer: a dawn for evolutionary medicine. Annu. Rev. Genet. *39*, 359–407.

Zhang, L., Guo, X.Q., Chu, J.F., Zhang, X., Yan, Z.R., and Li, Y.Z. (2015). Potential hippocampal genes and pathways involved in Alzheimer's disease: a bioinformatic analysis. Genet. Mol. Res. *14*, 7218–7232.

Zhang, M., Deng, Y.N., Zhang, J.Y., Liu, J., Li, Y.B., Su, H., and Qu, Q.M. (2018). SIRT3 protects rotenone-induced injury in SH-SY5Y cells by promoting autophagy through the LKB1-AMPK-mTOR pathway. Aging Dis. *9*, 273–286.

Zhang, X., Yuan, Z., Zhang, Y., Yong, S., Salas-Burgos, A., Koomen, J., Olashaw, N., Parsons, J.T., Yang, X.J., Dent, S.R., et al. (2007). HDAC6 modulates cell motility by altering the acetylation level of cortactin. Mol. Cell *27*, 197–213.

Zhang, Y., Kwon, S., Yamaguchi, T., Cubizolles, F., Rousseaux, S., Kneissel, M., Cao, C., Li, N., Cheng, H.L., Chua, K., et al. (2008). Mice lacking histone deacetylase 6 have hyperacetylated tubulin but are viable and develop normally. Mol. Cell. Biol. *28*, 1688–1701.

Zhong, Z., Tao, Y., and Yang, H. (2015). Treatment with harmine ameliorates functional impairment and neuronal death following traumatic brain injury. Mol. Med. Rep. *12*, 7985–7991.

iScience, Volume *24*

Supplemental information

Acetylation of NDUFV1 induced by a newly synthesized HDAC6 inhibitor HGC rescues dopaminergic neuron loss in Parkinson models

Bing Li, Yinuo Yang, Yuejun Wang, Jing Zhang, Jie Ding, Xiaoyu Liu, Yan Jin, Bolin Lian, Yong Ling, and Cheng Sun

Supplemental Information

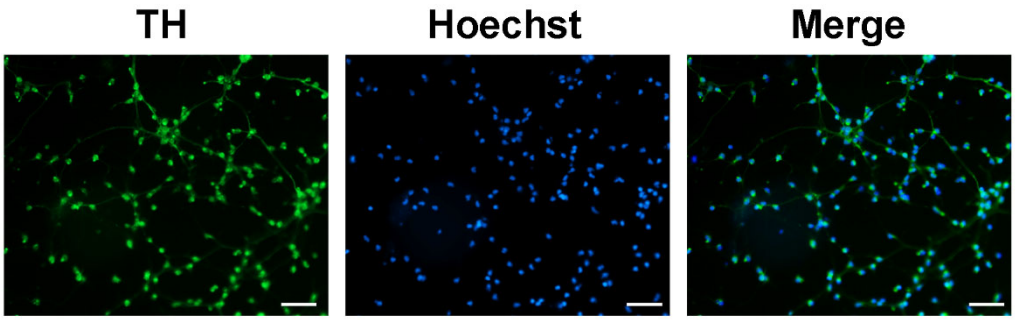

Figure S1. Related to Figure 3. Characterization of primary dopaminergic neurons. Primary dopaminergic neurons were analyzed by immunofluorescence staining using anti-TH antibody. Nuclei were identified by Hoechst. Scale bar = 50 μm.

Transparent Methods

Preparation of HGC

L-tryptophan (Purity ≥ 98%), 4-methoxybenzaldehyde (Purity ≥ 98%), harmine (Purity ≥ 98%), vorinostat (SAHA, Purity ≥ 99%), and compounds 1, 2, 5 (Purity ≥ 98%) were purchased from Aladdin Technologies Inc. (Shanghai, China). Compounds 3 and 4 were synthesized according to the procedures described elsewhere (Ling et al., 2018). ^{1}H NMR spectra were recorded with a Bruker Advance 400 MHz spectrometer at 300 K, using TMS as an internal standard. MS spectra were recorded on a Mariner Mass Spectrum (ESI). High resolution mass spectra (HRMS) were recorded using an Agilent Technologies LC/MSD TOF. All compounds were routinely checked by TLC and ^{1}H NMR. TLCs and preparative thin-layer chromatography were performed on silica gel GF/UV 254, and the chromatograms were conducted on silica gel (200-300 mesh, Merck) and visualized under UV light at 254 and 365 nm. All solvents were reagent grade and, when necessary, were purified and dried by standard methods. Solutions after reactions and extractions were concentrated using a rotary evaporator operating at a reduced pressure of ca. 20 Torr. Organic solutions were dried over anhydrous sodium sulfate. All compounds were of >95% purity determined by HPLC.

The purity of HGC

High-performance liquid chromatography (HPLC) analysis methods: column: Shimadzu C18 (150 mm × 4.6 mm × 5 μm); mobile phase: methanol: water = 75:25; wavelength: 254 nm; flow rate: 1 ml/min.

HDAC activity assay

The procedures for HDAC activity assay were described elsewhere (Thakur et al., 2020). Briefly, HGC and SAHA (Sigma-Aldrich; SML0061) were dissolved in DMSO to specific concentration, which were then prepared into serial dilutions. Recombinant HDAC proteins including HDAC1 (Active Motif; Catalog: #31504), HDAC2 (Active Motif; Catalog: #31505), HDAC4 (Active Motif; Catalog: #31364), HDAC6 (Active Motif; Catalog#: 31543), and HDAC8 (Active Motif; Catalog: #31536) were added into HDAC reaction buffer (50 mM Tris-HCl, pH 8.0, 2.7 mM KCl, 137 mM NaCl, 1.0 mM $MgCl_2$, 1 mg/ml BSA). Testing compounds were delivered into enzyme mixture.

Substrate for HDAC 1/2/6/8 (Sigma-Aldrich; Catalog: #SRP0306) or HDAC 4 (Sigma-Aldrich; Catalog: #SRP0303) was added to initiate deacetylation reaction with 1 h-incubation at 30°C. At the end of reaction, the developer solution containing Trichostatin A (BPS Bioscience; Catalog: #50030) was added to stop the reaction. Fluorescence was recorded in a microplate reader (BioTek, USA) with excitation at 360 nm and emission at 460 nm. IC50 values were calculated using the GraphPad (Prism 4) software.

Plasmids

pMito Timer was a gift from Zhen Yan (Addgene; plasmid: #52659; http://n2t.net/addgene:52659; RRID: Addgene_52659) (Laker et al., 2014). The coding sequence of *Ndufv1* was synthesized and incorporated into pcDNA3.1 vector by using restriction enzyme sites of Hind Ⅲ and BamH I. NDUFV1 K28R was generated by a PCR-based mutagenesis kit (Stratagene, La Jolla, CA) using pcDNA3.1-NDUFV1 as a template. The primer sequences are: 5'-ACGACAGCACCCAGGAAAACCTCATTTGGCTCAC-3' (forward) and 5'-CCAAATGAGGTTTTCCTGGGTGCTGTCGTGCC-3' (reverse). All the plasmids were verified by sequencing.

Ndufv1 knockdown

Three pairs of siRNAs targeting *Ndufv1* were synthesized at Ribobio (Guangzhou, China). The sequences of siRNAs were: GGTGACTGGTACAAGACAA (siRNA-1#); CGCGCTGCCTATATCTACA (siRNA-2#); CAAGGACCGGGAGATCTTA (siRNA-3#). For gene knockdown, the siRNAs against *Ndufv1* were transfected into SH-SY5Y cells for 72 h. Total RNA and cell lysates were prepared respectively for evaluating knockdown efficiency by using qRT-PCR and western blot.

Cell culture and treatments

SH-SY5Y cells were obtained from ATCC (Manassas, VA, USA). Cells were cultured in DMEM supplemented with 10% fetal bovine serum (FBS), and incubated at 37°C in a humidified atmosphere with 5% CO_2. Primary rat dopaminergic neurons were prepared according the methods described elsewhere (Peng et al., 2018). Briefly, neurons were cultured in neurobasal

medium supplemented with 2% B27. The maturation of mesencephalic neurons required 7-8 days with medium changes every 2 days. Cells were pretreated with HGC at different dosages (0.25, 0.5 and 1.0 μM). After 6 h-pretreatment, primary dopaminergic neurons and SH-SY5Y Cells were treated with 50 μM and 500 μM of MPP^+ for 24 h, respectively.

Cell viability assay

MTT assay was employed for cell viability assay. Briefly, cells were seeded in 96-well plates at 1×10^4 cells per well. At the end of treatments, cell culture medium was removed and a final concentration of 500 μg/ml of MTT was added to each well. After 4 h-incubation at 37°C, cells were harvested in 10% SDS and cell lysates were incubated at 37°C for 20 h. Absorbance at 570 nm was measured with a microplate reader (BioTek, USA).

LDH assay

LDH activity was measured by a commercial kit according to the manufacturer's instructions. Briefly, at the end of treatments, cell culture medium was harvested and then incubated with the LDH-assay reaction mixture. The incubation was performed for 30 min at room temperature in dark. The absorbance at 490 nm was detected with a microplate reader (BioTek, USA). Cell death ratio was calculated by the formula: The cell death ratio (%) = $(A_{sample} - A_{blank})/(A_{max} - A_{blank}) \times 100$.

Mitochondrial membrane potential assay

Mitochondrial membrane potential (MMP) was analyzed with a JC-1 staining kit according the manufacturer's instructions. Briefly, 5 μg/ml of JC-1 was added into each well and incubation was conducted at 37°C for 20 min in dark. After incubation, cells were washed with cold PBS buffer for three times. Absorbance at 590 nm represents high membrane potential (red color), and absorbance at 530 nm represents low membrane potential (green color). Images were collected using a fluorescence microscope (IX73, Olympus, Japan). The fluorescence intensity was quantified by the Image J software. The average fluorescence intensity was calculated from 10 regularly distributed areas in each image.

Mitochondrial function analysis

SH-SY5Y cells were cultured on glass coverslips in DMEM with high glucose containing 10% FBS and maintained at 37°C with 5% CO_2. The procedures for mitochondrial function analysis were described elsewhere (Laker et al., 2014). In brief, cells were transfected with pMito Timer (Addgene; Plasmid: #52659) using Lipofectamine (Invitrogen; Catalog: #11668019). 12 h-post transfection, cells were subjected to the treatments with HGC and MPP^+ as indicated in each Figure legend. After the treatments, cells were washed with PBS twice and fixed with 4% paraformaldehyde for 15 min on ice. Images were acquired by a confocal microscopy (Zeiss, LSM880) for both green (excitation/emission 488/518 nm) and red channels (excitation/emission 543/572 nm). The fluorescence intensity was quantified using the Image J software.

Co-immunoprecipitation

Cells were lysed in RIPA buffer containing 50 mM Tris (pH7.4), 150 mM NaCl, 0.5% NP-40, 0.5% sodium deoxycholate, 1 mM EDTA, 1 mM Na_3VO_4, 10 μg/ml Leupeptin, 10 μg/ml Aprotinin and 2 mM PMSF. Lysates were centrifuged at 12,000 rpm for 20 min at 4°C. The supernatant was subjected for protein concentration analysis by using Protein Assay Kit (Bio-Rad). Lysates containing 1 mg total protein were incubated with 1 μg of anti-NDUFV1 antibody for 10 h at 4°C. After incubation, protein A agarose beads (Millipore; Catalog: #16-156) were added and incubated for additional 2 h. Agarose beads were precipitated after centrifugation and supernatants were discarded. After thoroughly washing, 2X loading buffer was added to the resulting beads and boiled at 100°C for 5 min. The immuno-complex samples were analyzed by western blot.

Animals

To generate Parkinson's disease model mice, 8-week-old male C57BL/6J mice were treated with MPTP (20 mg/kg) via intraperitoneal injection (i.p.) at 24-h interval, for 7 consecutive days. The control mice were injected with saline. The saline group and MPTP group were randomly divided into two groups (n = 5 for each group). HGC was delivered to mice (i.p.) at the dosage of 50 mg/kg/day for 7 days. The dosage of HGC was selected based on previous reports, in

which other HDAC inhibitors were administered to mice to treat central nervous system disorders (Chopra et al., 2016; Guan et al., 2009; Sharma and Taliyan, 2016). All the animal protocols were approved by the Committee of Nantong University and the Administration Committee of Experimental Animals, Jiangsu Province, China (Approval ID: SYXK [SU] 2017-0046).

Behavioral tests

Rotarod test was performed using an accelerating rotarod apparatus (model LE8500; Panlab) (Choi et al., 2013). The mice were trained for 2 consecutive days before MPTP injections in an acceleration mode (4-40 rpm) over 5 min. The training was repeated with a constant speed (16 rpm) until the mice were able to stay on the rod for at least 300 s. For the formal test, mice were placed on a rotating drum, accelerated from 4 to 40 rpm over a 5 min period. Time spent moving on the rod was recorded before falling was measured. Pole test was conducted with the method described elsewhere (Choi et al., 2013). Briefly, mice were held on the top of a pole (diameter 16 mm; height 60 cm) with a rough surface. Mice were habituated to the task 1 d before testing. On the test day, the total time taken to descend was measured and considered as locomotion activity. For tail suspension test, mice were suspended by the tail for 10 min so that the hindlimbs were elevated and forelimbs were allowed to touch the floor of the cage. Immobility was scored as total time spent in a behavioral state devoid of head and limb movement. Episodes of immobility were counted toward the total if they occurred after the first minute of tail suspension and lasted for 5 s or longer. The data were recorded by SMART Video Tracking System (RWD, Shenzhen, China) and analyzed by the accompanied software (Smart V3.0). For olfactory test, mice were fed with cheese pellets before olfactory test to make sure they are familiar with the pellet odor. Mice were fasted for 20 h prior to the test. One cheese pellet was buried 1.0 cm below the bedding on a corner of cage. In each test, mouse was placed at the center of cage at the beginning. The time was recorded when the cheese pellet was detected and eaten by mice. If mouse failed to find the pellets within 5 min, the test stopped and a score of 300 s was awarded.

Tissue collection and preparation

Mice were perfused transcardially with ice-cold PBS (0.1 M, pH7.4) after deep anesthesia with isoflurane. The brains were immediately extracted and cut sagittally into hemispheres. For immunofluorescence and immunohistochemistry analysis, one hemisphere was fixed overnight in 4% PFA and then dehydrated in 10% and 30% sucrose in PBS at 4°C. The other hemisphere was further dissected into the SNpc and striatum under stereomicroscopy according to mouse brain atlas. For gene expression analysis, the collected SNpc and striatum were immediately frozen in liquid nitrogen and kept at -80°C freezer until use.

Immunohistochemistry, Nissl staining and stereological estimation

The coronal sections at approximately 3.28 mm behind (-2.54 ~ -4.04 mm) the bregma were used for analyzing dopaminergic neurons in the SNpc (Paxinos, 2001). The sections at approximately 0.62 mm ahead (0.98 ~ 0.50 mm) of the bregma were sampled for assessing density of striatal TH-positive nerve fibers (Paxinos, 2001). The fourth and fifth 30 μm-thick sections were used for analyzing TH-positive cell numbers in the SNpc. Tissues were fixed in phosphate-buffered 4% paraformaldehyde, pH 7.4, at 4°C. Fixed tissue sections were then incubated overnight with mouse anti-tyrosine hydroxylase (TH) at 4°C. They were then incubated with biotinylated anti-mouse IgG for 1 h followed by 1 h-incubation in ABC solution at 37°C. The peroxidase activity was visualized with DAB in 50 mM tris-buffered saline (pH 7.6). For Nissl staining, paraffin sections were deparaffinized and hydrated, stained with methylene blue buffer for 10 min and then immersed into acetic acid buffer for 2 min. Pictures were taken using a light microscopy (Leica, DM2500 LED). The total numbers of TH- and Nissl-positive cells were counted by unbiased stereology method as described elsewhere (Alam et al., 2017; Nam et al., 2015). TH immunoreactivity in the striatum was analyzed by measuring density of TH signal using ImageJ software (National Institutes of Health, Bethesda, MD, USA).

Transmission electron microscope analysis

The SNpc samples were fixed in cacodylate buffer (0.1 M, pH 7.4) containing 2.5% glutaraldehyde and 2.5% paraformaldehyde. Post-fixation, the samples were immersed in 1% osmium tetraoxide at 4°C for 1 h, and then samples were dehydrated using graded alcohol (50, 70, 90 and 100%). Ultrathin sections were cut at 70 nm and contrasted with uranyl acetate and

lead citrate, and examined at 80 kv with a transmission electron microscope (JEO Ltd., Tokyo, Japan) at various magnifications by a blinded investigator.

RNA extraction and quantitative real time PCR (qRT-PCR)

Total RNA was extracted from cells using Trizol reagent (Invitrogen) and transcribed into cDNA using cDNA synthesis kit (Bio-Rad). Gene expression analysis was performed with iQ5 Multicolor Real-Time PCR Detection System (Bio-Rad) with SYBR Green Supermix (Bio-Rad). The mRNA level was calculated by the $2^{-\triangle\triangle CT}$ method and normalized to the expression of 18S. The primer sequences used were: *Ndufv1*, 5'-TTT CTC GGC GGG TTG GTT C-3' (forward) and 5'-GGT TGG TAA AGA TCC GGT CTT C-3' (reverse); 18S, 5'- AGT CCC TGC CCT TTG TAC ACA-3' (forward) and 5'- CGT TCC GAG GGC CTC ACT-3' (reverse); *Nd1*, 5'-GTT GGT CCA TAC GGC ATT TT-3' (forward); 5'-TGG GTG TGG TAT TGG TAG GG-3' (reverse); *Ppia,* 5'-GCA TAC GGG TCC TGG CAT CTT GTC C-3' (forward); 5'-ATG GTG ATC TTC TTG CTG GTC TTG C-3' (reverse).

Protein extraction and western blot analysis

Tissue protein extraction was described elsewhere (Liu et al., 2016). Briefly, tissues were homogenized with a bench-top homogenizer (Polytron, PT2100) in ice-cold tissue lysis buffer (25 mM Tris-HCl, pH 7.4; 100 mM NaF; 50 mM $Na_4P_2O_7$; 10 mM Na_3VO_4; 10 mM EGTA; 10 mM EDTA; 1% NP-40; 10 µg/ml Leupeptin; 10 µg/ml Aprotinin; 2 mM PMSF and 20 nM Okadaic acid). After homogenization, lysates were subjected to centrifugation at 12,000 rpm for 20 min at 4°C. Protein concentration was quantified by using Protein Assay Kit (Bio-Rad). The lysates were cooled to room temperature for western blot analysis (Sun et al., 2014). Samples were resolved by SDS-PAGE and then transferred to polyvinylidene fluoride (PVDF) membrane. After 1 h blocking at room temperature using 10% blocking reagent (Roche), membrane was incubated overnight with primary antibody (1:1000 dilution) in Tris-buffered saline solution/Tween (TBST) containing 10% blocking reagent at 4°C. Membrane was then washed three times in TBST and incubated with the secondary antibody (1:10,000 dilution) for 1 h at room temperature. After three-time washing in TBST, membrane was developed using a chemiluminescence assay system (Roche) and exposed to Kodak films. Blots were quantified

by the Image J program.

ETC complex I activity assay

Mitochondria were isolated from SH-SY5Y cells by using a mitochondria isolation kit (Sigma-Aldrich, MITOISO2). ETC complex I activity was assayed with a mitochondrial Complex I activity assay kit (Sigma-Aldrich, MAK359) according to the manufacturer's protocol. Briefly, 2 μl of mitochondrial samples (1-5 μg) were added to wells containing sample mix, in which 57 μl of Complex I assay buffer, 2 μl of decylubiquinone and 9 μl of Complex I dye were included. 30 μl of 1X NADH working solution was added to each well and then the plate was read immediately at 600 nm for 5 min with a microplate reader (BioTek, USA) at room temperature. One unit of Complex I is the amount of enzyme that will cause reduction of 1.0 μmol of the dye per minute at pH7.4 at room temperature.

Statistical analysis

Data are presented as means ± SEM. All experiments were undertaken in triplicates. Statistical significance was calculated with one-way ANOVA with Bonferroni's *post hoc* test. Significance was accepted at the level of $P < 0.05$.

Supplemental References

Alam, G., Edler, M., Burchfield, S., and Richardson, J.R. (2017). Single low doses of MPTP decrease tyrosine hydroxylase expression in the absence of overt neuron loss. Neurotoxicology *60*, 99-106.

Choi, D.Y., Lee, M.K., and Hong, J.T. (2013). Lack of CCR5 modifies glial phenotypes and population of the nigral dopaminergic neurons, but not MPTP-induced dopaminergic neurodegeneration. Neurobiol. Dis. *49*, 159-168.

Chopra, V., Quinti, L., Khanna, P., Paganetti, P., Kuhn, R., Young, A.B., Kazantsev, A.G., and Hersch, S. (2016). LBH589, A Hydroxamic Acid-Derived HDAC Inhibitor, is Neuroprotective in Mouse Models of Huntington's Disease. J. Huntingtons Dis. *5*, 347-355.

Guan, J.S., Haggarty, S.J., Giacometti, E., Dannenberg, J.H., Joseph, N., Gao, J., Nieland, T.J., Zhou, Y., Wang, X., Mazitschek, R., et al. (2009). HDAC2 negatively regulates memory formation and synaptic plasticity. Nature *459*, 55-60.

Laker, R.C., Xu, P., Ryall, K.A., Sujkowski, A., Kenwood, B.M., Chain, K.H., Zhang, M., Royal, M.A., Hoehn, K.L., Driscoll, M., et al. (2014). A novel MitoTimer reporter gene for mitochondrial content, structure, stress, and damage in vivo. J. Biol. Chem. *289*, 12005-12015.

Ling, Y., Guo, J., Yang, Q., Zhu, P., Miao, J., Gao, W., Peng, Y., Yang, J., Xu, K., Xiong, B., et al. (2018). Development of novel beta-carboline-based hydroxamate derivatives as HDAC inhibitors with

antiproliferative and antimetastatic activities in human cancer cells. Eur. J. Med. Chem. *144*, 398-409.

Liu, X., Zhao, Y., Peng, S., Zhang, S., Wang, M., Chen, Y., Zhang, S., Yang, Y., and Sun, C. (2016). BMP7 retards peripheral myelination by activating p38 MAPK in Schwann cells. Sci. Rep. *6*, 31049.

Nam, J.H., Park, E.S., Won, S.Y., Lee, Y.A., Kim, K.I., Jeong, J.Y., Baek, J.Y., Cho, E.J., Jin, M., Chung, Y.C., et al. (2015). TRPV1 on astrocytes rescues nigral dopamine neurons in Parkinson's disease via CNTF. Brain *138*, 3610-3622.

Paxinos, G., Franklin, K. (2001). The Mouse Brain in Stereotaxic Coordinates. (New York: Academic Press).

Peng, S., Xu, L., Ma, J.Y., Gu, X.S., and Sun, C. (2018). Achyranthes bidentata polypeptide protects dopaminergic neurons from apoptosis induced by rotenone and 6-hydroxydopamine. Neural Regen. Res. *13*, 1981-1987.

Sharma, S., and Taliyan, R. (2016). Epigenetic modifications by inhibiting histone deacetylases reverse memory impairment in insulin resistance induced cognitive deficit in mice. Neuropharmacology *105*, 285-297.

Sun, C., Wang, M., Liu, X., Luo, L., Li, K., Zhang, S., Wang, Y., Yang, Y., Ding, F., and Gu, X. (2014). PCAF improves glucose homeostasis by suppressing the gluconeogenic activity of PGC-1alpha. Cell Rep. *9*, 2250-2262.

Thakur, A., Tawa, G.J., Henderson, M.J., Danchik, C., Liu, S., Shah, P., Wang, A.Q., Dunn, G., Kabir, M., Padilha, E.C., et al. (2020). Design, Synthesis, and Biological Evaluation of Quinazolin-4-one-Based Hydroxamic Acids as Dual PI3K/HDAC Inhibitors. J. Med. Chem. *63*, 4256-4292.